Temperature and precipitation regime in LGM human refugia of southwestern Europe inferred from δ13C and δ18O of large mammal remains

Christophe Lécuyer, Claude Hillaire-Marcel, Ariane Burke, Marie-Anne Julien, Jean-François Hélie

Temperature and precipitation regime in LGM human refugia of southwestern Europe inferred from $\delta^{13}C$ and $\delta^{18}O$ of large mammal remains

Christophe Lécuyer[1,*], Claude Hillaire-Marcel[2], Ariane Burke[3], Marie-Anne Julien[4], Jean-François Hélie[2]

[1]Univ Lyon, Univ Lyon 1, ENSL, CNRS, LGL-TPE, 69622 Villeurbanne, France

[2]Geotop-UQAM, CP 8888, Montréal, QC, H3C 3P8, Canada

[3]Université de Montréal, Département d'Anthropologie, C.P. 6128, Centre-Ville, Montréal, QC, H3C 3J7, Canada

[4] Independent researcher.

*corresponding author: Christophe.lecuyer@univ-lyon1.fr

Abstract – The climate shift of the Last Glacial Maximum (LGM) strongly impacted the vegetation cover and related trophic chains of western Europe. Harsh, cold and dry conditions then prevailed in most regions, strongly impacting migrations and survival of human beings. Nonetheless, environments suitable for mammalian fauna to survive persisted in SW Europe thus providing refugia for hunters. Tooth enamel from large herbivorous mammal remains from archeological sites located in southwest France and Spain were analyzed for their stable carbon and oxygen isotope compositions for documenting paleotemperatures and paleoprecipitations. These sites were occupied by humans between 25 ky and 16 ky. Skeletal remains of Cervidae, Equidae and Caprinae suggest colder and drier conditions relative to present-day. Paleoprecipitations were reconstructed from a modern-based transfer function using $\delta^{13}C$-values of apatite carbonate, then corrected for the low atmospheric pCO_2 value of the LGM. They ranged from ≈250 mm yr^{-1} on the Mediterranean façade, to ≈550 mm yr^{-1} on the Atlantic side. Setting the $\delta^{18}O$-value of the northeastern North Atlantic LGM-surface water to +0.8‰, based on Biscay Golf marine core studies, mean air temperatures inferred from ^{18}O-data in apatite calcite were close to 14–15°C (Mediterranean) and 6°C to 10°C (Atlantic), i.e., about 4–5°C and 5–8°C higher than pre-industrial temperatures, respectively. The two areas thus define distinct clusters of air temperatures and precipitation regimes with strong negative offsets vs the Present. These isotopically-reconstructed climate conditions indicate a strong control from proximal surface ocean/marine waters, in particular of mean annual air temperatures.

Keywords: Last Glacial; temperature; precipitation; stable isotopes; apatite; mammals; Western Europe

43

44

45 1. Introduction

46 The Last Glacial, also named Weichselian in Northwest Europe, covers a time period
47 from 115 ka to 11.7 ka. It was characterized by rapid, large amplitude climatic fluctuations
48 recorded in the Greenland ice cores (Dansgaard et al., 1993; Grootes et al., 1993; NGRIP
49 members, 2004; Rasmussen et al., 2014) and North Atlantic marine sediments (Heinrich,
50 1988; Bond et al., 1992; Sanchez Goñi et al., 2008). During this period, global climate
51 conditions oscillated between stadial and interstadial conditions, sometimes punctuated by
52 abrupt climate events known as Heinrich events. These highly contrasted climate regimes
53 influenced faunal communities, including humans, through the development of new migration
54 pathways, allopatric speciation in refugia, and enhanced rates of extinction during the coldest
55 and driest stages of the Last Glacial.

56 The Last Glacial Maximum (LGM), conventionally dated between 23 and 19 ka ago
57 (MARGO, 2009; Mix et al., 2001), is defined as the most recent period of maximum global
58 ice volume (Mix et al., 2001). It featured lowered greenhouse gas (CH_4, CO_2) concentrations,
59 a mean sea level ~120 m lower than today and generally cold and dry climatic conditions
60 resulting in significant modifications of both floral and faunal assemblages (Lister, 2004;
61 Sommer and Nadachowski, 2006; Clark et al., 2009; Binney et al., 2017; Cao et al., 2019).
62 During this interval, and in response to global tropospheric cooling, the Northern Hemisphere
63 experienced a southward expansion of continental ice sheets, which reached as far as 52°N in
64 western Europe. Various models suggest a decrease in global mean surface air temperatures
65 during the LGM ranging from 4°C to 10°C vs pre-industrial (PI) climatic conditions (Masson-
66 Delmotte et al., 2006; Schneider von Deimling et al., 2006; Annan and Hargreaves, 2013).
67 The main causes of this decrease are thought to be the combined effect of lower atmospheric

CO_2 values (with a partial pressure as low as 190 ppm; Bouttes et al., 2011) and ice-sheet forcing, which would jointly account for about 75% of the total LGM cooling (Schneider von Deimling et al., 2006). Additional cooling effects are related to changes in atmospheric dust content and vegetation cover. In response to this maximal extent of continental ice (glaciers and ice caps), mean global sea level dropped by 120±10 m (Lambeck et al., 2014).

Faunal associations described in the archaeological sites of southwestern Europe are generally compatible with cold and dry, open environments, such as tundra and dry steppe, but there are important regional differences as suggested by Yravedra and Brugal (2005) who defined several biogeographic zones in southwest Europe. During the LGM, the vegetation in Europe was characterized by an expansion of tundra and steppe. In Southwestern France and in the northern part of the Iberian Peninsula, cold temperate fauna (horse, reindeer, ibex) dominated vertebrate assemblages during the LGM, but co-existed with cold-adapted fauna such as mammoth, woolly rhinoceros and reindeer (Yravedra and Brugal, 2005; Sommer and Nadachowski, 2006; Álvarez-Lao and García, 2011; Álvarez-Lao and García, 2011). Recent models suggest that the most suitable habitats for humans during the LGM were concentrated in southwest France and the Iberian Peninsula, excluding the interiors, as also demonstrated by the distribution of archaeological sites (e.g., Ludwig et al., 2018; Burke et al., 2017; Wren and Burke, 2019). Modern humans who had arrived in Europe ≈ 45,000 years ago survived the LGM in the SW Europe refugia (Fu et al., 2016). A post-ice age expansion followed, with their descendants spreading out in Iberia, after ≈ 19,000 years ago, then defining the Magdalenian culture (Fu et al., 2016).

The LGM in Southwest Europe illustrates a major faunal and vegetation partitioning in biogeographic provinces, which constrained the human strategy of land occupation. Whether Mean Annual Precipitation (MAP) or Mean Annual Air Temperature (MAAT) were limiting factors in this strategy remains to be fully elucidated. In thus study, special attention is paid to

93 sites from coastal areas under the influence of the Atlantic Ocean or the Mediterranean Sea.
94 They represent three distinct biogeographic zones, following the classification of Yravedra
95 and Brugal (2005) for southwestern Europe: southwest France (zone VI), Cantabria/Asturias
96 (zone IV) and the Mediterranean coast (zone IIIa).

97 MAAT and MAP may be reconstructed using oxygen and carbon isotope compositions of
98 the apatite carbonate from vertebrate skeletons. As highlighted by Pederzani and Britton
99 (2019), in particular the oxygen isotope analyses of skeletal remains ($\delta^{18}O$) are a powerful
100 tool for exploring past human-environment interactions as well as to reconstruct paleoclimatic
101 parameters. An approach not yet used for documenting the LGM refugia of SW Europe will
102 fill this gap using large mammal remains (teeth) from the above defined human occupation
103 areas. We also intend to demonstrate that carbon isotope ($\delta^{13}C$) from such remains may
104 inform specifically on paleoprecipitation.

105 The basic principles to interpret $\delta^{13}C$ as MAP and $\delta^{18}O$ as MAAT are summarized as
106 follows:

107 The most common strategy consists in estimating air temperature from the oxygen isotope
108 composition of the carbonate or the phosphate groups of the tooth enamel of the vertebrate
109 apatite. During tooth growth, the oxygen isotope composition of apatite carbonate ($\delta^{18}O_c$)
110 records body temperature (a near constant close to 37°C) and body water composition
111 ($\delta^{18}O_{bw}$) (Koch et al., 1989; Bryant et al., 1996; Chenery et al., 2012). The oxygen isotope
112 composition of body water reflects that of meteoric water (Bryant and Froelich, 1995; Kohn,
113 1996; Langlois et al., 2003) and depends principally on the composition of oceanic moisture
114 source(s), the length and precipitation history of humid air mass trajectories,
115 evapotranspirative processes along these trajectories, air temperature (MAAT) during
116 precipitation, the relative amount of precipitation and altitude relative to sea level (Dansgaard,
117 1964; Rozanski et al., 1992; Fricke and O'Neil, 1999). At mid- and high-latitudes (tropical

bands excluded), MAAT of areas close to oceanic moisture sources are linearly related to the weighted mean annual $\delta^{18}O_{mw}$ (Dansgaard, 1964; Yurtsever, 1975; von Grafenstein et al., 1996; Fricke and O'Neil, 1999; Skrzypek et al., 2011; Lécuyer, 2013). This property of the water cycle has already been used for the reconstruction of past air temperatures from the oxygen isotope composition of vertebrate tooth enamel from large mammals (e.g., Ayliffe et al., 1992; Bryant et al., 1994; Tütken et al., 2007; Bernard et al., 2009; Fabre et al., 2011).

The reconstruction of MAP from the carbon isotope composition of apatite carbonate was made in several steps. In the first step, the $\delta^{13}C$ values of plants ($\delta^{13}C_{pl}$) can be estimated from tooth enamel carbonate ($\delta^{13}C_{carb}$) taking into account the isotopic fractionation that takes place between diet-derived carbon ingested by the herbivores and the carbon mineralized as carbonate present in the apatite crystal lattice of their teeth (Tejada-Lara et al., 2018). In a second step, MAP values are calculated using $\delta^{13}C_{pl}$ and a transfer function based on plant leaf discrimination factors (Kohn, 2010) that may be estimated in the case of animal diets strictly based on Calvin Cycle (C3) plants. Atmospheric pCO_2-changes and reduced biomass production by plants during glacials (Gerhart and Ward, 2010) may have led to some global relative increase in the abundance of C4 plants, thus to some possible dietary changes, but C3/C4 plant ratios within given biomes remained broadly stable if biome distributions differed (Ehleringer, 2005). Moreover, C4 plants amount to only about 1% in the European vegetation (Collins and Jones 1985). They are slightly more abundant in herb-dominated biomes (see their taxonomic distribution in Pyankov et al. (2010). Now, if such biomes experienced a ~ 10% relative increase over other biomes during the LGM (Binney et al., 2017), their content in C4 plants is unlikely to have increased as these plants are strongly sensitive to temperatures (Pyankov et al., 2010), adding to the equivocal response of the C4/C3 plant ratio of Poaceae, one of their major components, to pCO_2 changes (Wand et al.,

142 1999). One may thus assume a nearly exclusive C3-plant vegetation during the LGM interval
143 whatever the changes in biome distribution.
144 The goal of the present study is thus to build paleoclimate reconstructions for several
145 archaeological sites of the LGM (Figure 1) using the above isotopic approaches. The specific
146 sampled sites are Laugerie-Haute (Dordogne, France), El Cierro (Asturias Province), Hornos
147 de la Peña, El Pendo and El Ruso (Cantabria Province), Nerja (Málaga Province) and
148 Malladetes (Valencia Province). The present study provides the first quantitative information
149 about LGM-MAAT and -MAP ranges of these sites. They will be discussed in the light of
150 proxies based on pollen assemblages (continental climate) and foraminiferal-$\delta^{18}O$ data
151 (marine moisture sources), climatic model outputs, past topography, as well as in that of
152 reconstructed vegetation cover and faunal communities.
153
154 2. Archaeological sites and sample collection
155 2.1. Description of the sampled archaeological sites
156 *Laugerie Haute Est* (LHE) forms part of a much larger rock-shelter on the right bank of
157 the Vézère river in the Dordogne region of France (Fig. 1). The shelter, which is about 30 m
158 deep and 180 m long, is separated into two excavated sections (East and West) due to the
159 presence of a house occupying the centre of the shelter. First discovered at the end of the 19th
160 Century the site's stratigraphic integrity has come under close scrutiny (Texier, 2009;
161 Delpech, 2012; Verpoorte et al., 2019). The occupation sequence of the site spans the
162 Aurignacian and the Solutrean. For this study, level 4-8, attributed to Magdalenian II, level
163 10-16 (F. Bordes collection) attributed to Magdalenian I and level 18-20, attributed to
164 Magdalenian 0, were sampled. Biostratigraphically, levels attributed to Magdalenian I-III
165 form a unit, with faunal assemblages dominated by reindeer, while the Magdalenian 0 level,
166 which is dominated by horse, is distinct (Delpech, 2012). The Magdalenian levels are

167 bracketed by ages of ~ 23 and ~21 ^{14}C cal. kyr (Delpech, 2012) and can thus be assigned to
168 the LGM. Four sites were sampled in northern Spain, including: El Ruso, Hornos de la Peña
169 and El Pendo in Cantabria, and El Cierro in Asturias (Fig. 1). El Ruso is a small cave located
170 about 6 km from the modern coastline, near El Pendo and El Juyo (unsampled). The cave
171 contains a sequence of occupation that spans from the Mousterian to the Solutrean Level 3,
172 the Upper Solutrean level sampled here overlies a Solutrean level (IV) dated 20–19 ^{14}C cal.
173 kyr (Yravedra, 2010a).

174 At El Pendo level 4, the samples are labelled "level 4" and attributed to the Upper
175 Solutrean. If this corresponds to level IV (Eschegaray excavations) this level is attributed to
176 the Late Aurignacian, although it is intercalated between Gravettian and Magdalenian levels
177 (Hoyos Gómez and Laville, 1982). Unfortunately, the stratigraphic integrity of this site is in
178 some doubt (de los Terreros and Castanedo, 2010; Barquin, 2014). Consequently, results from
179 this site must be interpreted with caution.

180 At Hornos de la Peña, we sampled level B. This level is dated 23–21 ^{14}C cal. kyr and is
181 attributed to the Aurignacian in its lower part, and the Solutrean in its upper part (Breuil and
182 Obermeier, 1912 cited in Tejero et al., 2008; Yravedra, 2010b). The faunal assemblage at
183 Hornos de la Peña is dominated by horse (Tejero et al., 2008). At El Cierro (Asturias),
184 another deeply stratified cave site excavated by several different teams over the years, a
185 revised chronostratigraphy and several AMS dates are available (Alvarez-Fernandez et al.,
186 2016). We sampled levels G (Magdalenian), G1 and H (Solutrean) which form part of the
187 earliest occupation sequence of the cave. AMS dates obtained for these levels indicate that the
188 site was occupied during the LGM (^{14}C cal. ages of 20–19 kyr) (Alvarez-Fernandez et al.,
189 2016).

190 Two sites on the Mediterranean seaboard of Spain were sampled: Nerja and
191 Malladetes (aka Mallaetes) (Fig. 1). Nerja, the southernmost sample site, is a deeply stratified

192 cave located on the coastal plain of eastern Andalusia. The site contains one of the longest
193 occupation sequences in Mediterranean Spain, spanning the Gravettian to the Copper Age
194 (Aura Tortosa et al., 2006; Jordá Pardo and Aura Tortosa, 2008). Paleoclimate proxies and a
195 large number of recently reviewed radiocarbon dates provide a robust chronostratigraphic
196 frame for the sequence (Jordá Pardo and Aura Tortosa, 2008). Unit 8 (vestibule) was sampled
197 for this study. This unit contains Solutrean material and is generally considered to date to the
198 LGM, based on paleoclimate proxies and conventional and AMS radiocarbon dates yielding
199 ^{14}C cal. ages comprised between 23 and 21 kyr (Vallejo et al., 2005; Aura Tortosa et al.,
200 2006), although a much younger and possibly unrepresentative AMS date (≈ 14.4 ^{14}C cal.
201 kyr) has also been reported (Jordá Pardo and Aura Tortosa, 2008).
202 Malladetes (or Mallaetes) is located in the central Mediterranean region of Spain, in
203 Valencia. The levels sampled for this study include levels 7 (entrada D), 8 and 9 (entrada D)
204 which should be associated with the Gravettian (de la Peña Alonso, 2013). An AMS ^{14}C cal.
205 age of 30–26 kyr was obtained from modern human remains associated with unspecified
206 Gravettian levels in sector E, likely corresponding to levels VII to XI (Fortea Perez and Jorda
207 Cerda, 1976; Arsuaga et al., 2002), indicate that our samples probably predate the LGM and
208 level 8 at Nerja (Fumanal and Dupré, 1983; Aura Tortosa et al., 2006).
209
210 2.2. Sample collection
211 The samples recovered from the seven archaeological sites described above (Table 1)
212 include mammal remains assigned to Cervidae (*Cervus elaphus*, *Rangifer tarandus*), Equidae
213 (*Equus* sp.) and Caprinae (*Capra pyreneica*, *Rupicapra rupicapra, Saiga tatarica*). The
214 cervids (*Cervus elaphus*) and caprids (*Capra pyreneica*) were sampled as a priority, but
215 wherever these taxa were poorly represented, we sampled alternate species including smaller

cervids and small bovids. At Laugerie Haute Est and Hornos de la Peña we sampled horse remains because of their abundance at both sites.

2.3. Habitat and diet of Cervidae, Equidae and Caprinae

Cervus elaphus (red deer) is a large mammal observed in semi-open habitats, often found in forest margins and clearings, while it also occupied open environments such as steppes during the Last Glacial (Straus, 1981; Bugalho and Milne, 2003). It tolerates a wide range of temperature, as long as the habitat is not too dry. Its diet is highly eclectic and seasonally variable, although it shows a 60-70% herbaceous source. *Cervus elaphus* mainly browses leaves, conifer needles, twigs, nuts, shoots and bark of trees in winter, and grazes more on grasses, herbs, ferns, mosses, mushrooms, sedges or even rushes, during the summer and intermediate seasons.

Rangifer tarandus (reindeer) lives in subarctic and arctic regions (taiga and tundra), however some sub-species such as *R. tarandus tarandus* (woodland caribou) occupy the boreal forests (Ihl and Klein, 2001; Thompson et al., 2015) In winter, reindeers mainly feed on lichens which they access by digging holes in the snow cover. In the mild seasons, their diet is mainly based on grasses, green leaves of shrubs, tree bark and sedges as well as tree shoots such as larch, willow and birch. Mushrooms are also consumed during the late summer and early autumn.

Equus caballus (horse) was widely distributed in Eurasia and the Americas during the late Pleistocene. Equids are adapted to open habitats and are found in steppe, tundra and taiga habitats, as well as in more temperate grasslands. They are non-selective grazers and tolerate a wide range of temperatures (Berger, 1986).

Capra pyreneica (ibex) is a montane species living exclusively in open environments with high relief (cliffs and stone ravines; pastures in spring) at altitudes ranging from about

500 m to about 3500 m as observed in the Alps (Villaret et al., 1997). Its diet is essentially composed of herbaceous plants.

Rupicapra rupricapra (chamois) feeds on herbs and lives in mountains meadows and on the edge of forests. Chamois are well-adapted to rough terrain and tolerate a large range of temperatures as low as -20°C in winter and up to 25°C in summer (Christie, 1967; La Morgia and Bassano, 2009) although they are actually distributed in a wide range of temperate conditions.

Saiga tatarica (Eurasian antelope) feeds on salt-coated herbs, some grasses (Poaceae), Euphorbiaceae and Artemisia. This antelope lives in hilly areas and is considered an indicator of a dry climate (steppe environment) with highly-seasonally contrasted temperatures (Bekenov et al., 1998).

Among these large mammals, obligate to semi-obligate drinkers are horse (strict obligate drinker), red deer (drinks large amounts of water during the warm season), reindeer (free water in summer, snow during the cold season) whilst semi-obligate to non-obligate drinkers are ibex, chamois and antelope that drink free water occasionally (Macdonald, 2006).

3. Sample preparation and isotopic analysis

The tooth samples were prepared and analyzed at the Stable Isotopes Laboratory of the Geotop research center (Université du Québec à Montréal). Prior to any treatment, tooth crowns were mechanically cleaned to remove any trace of remaining glue or altered hard tissues. They were then immersed in an ultrasonic bath in order to eliminate potential remains of sedimentary particles. From 10 mg to 20 mg of enamel powder samples were collected using a micro-drill equipped with a diamond-studded drill bit. Grooves were drilled perpendicularly to the tooth growth axis from the cervix to the apex of the tooth crown.

Following the protocol used by Vigeant et al. (2017), organic matter was removed from tooth enamel apatite by soaking an aliquot of the untreated sample in a 2% sodium hypochlorite (NaOCl) solution for 24 h. Then, the samples were rinsed with large amounts of water, then dried before being treated with 1 M acetic acid-Ca acetate buffer (pH = 4.75) for 24h at 20°C to remove secondary carbonate phases (Bocherens et al., 1996), and finally washed with distilled water and dried at ambient temperature. For each sample, about 1 mg of enamel powder was analyzed for $\delta^{13}C$-values (‰ VPDB) and $\delta^{18}O$-values (‰VPDB) of the carbonate using a Micromass Isoprime™ isotopic ratio mass spectrometer operated in dual inlet mode and coupled to a Multicarb™ system. Overall analytical uncertainties ($\pm 1\sigma$) for $\delta^{13}C$ and $\delta^{18}O$ were close to 0.05‰ and 0.1‰, respectively, based on statistics from replicate measurement of samples, compared to ±0.02 and ±0.03‰, respectively, on reference carbonate materials (e.g., NBS 19, IAEA-603 and the home reference carbonate), thus suggesting some isotopic heterogeneity in the ground carbonate samples.

4. Results

The dataset is characterized by $\delta^{13}C$ and $\delta^{18}O$ values ranging respectively from -12.89‰ to -8.93‰ (mean = -10.42±0.76‰) and -8.65 to -0.14‰ (mean = -5.19±1.99‰). An examination of data compiled in Table 1 reveals that they form two distinct clusters corresponding to sites located on the Atlantic side and along the Mediterranean coast (Figure 1). As a first approach, pooling the taxa in each geographic cluster reveals that the $\delta^{18}O$ values of mammal remains from Nerja and Malladetes have much higher $\delta^{18}O$ values (-1.45±0.74) than those (-6.03±0.94) from the sites located on the Atlantic side (Table 1). The difference is not so striking for $\delta^{13}C$ values which average -10.60±0.70‰ in the Atlantic sites, i.e., slightly but significantly lower than that the mean value of Mediterranean sites, which is -9.65±0.44‰ (Welch t-test: $p = 4.4 \times 10^{-7}$; H_0 = means are equal).

290 Discrimination between the datasets increases further when distinguishing Cervidae from
291 Caprinae in the cluster of Atlantic sites, which removes a sampling bias as only Caprinae
292 were sampled in the Mediterranean sites. In the case of Cervidae, the distribution of data
293 satisfies the statistical criteria required by a normal distribution when using Shapiro-Wilk test
294 ($p = 0.30$ and $W = 0.963$ in the 95% critical range [0.937; 1.000] for $\delta^{13}C$ values; $p = 0.15$ and
295 $W = 0.953$ in the 95% critical range [0.937; 1.000] for $\delta^{18}O$ values). Similar conclusions are
296 obtained for the Caprinae when using Shapiro-Wilk test ($p = 0.50$ and $W = 0.964$ in the 95%
297 critical range [0.920; 1.000]) for $\delta^{13}C$-values; $p = 0.37$ and $W = 0.957$ in the 95% critical
298 range [0.920; 1.000] for $\delta^{18}O$-values).
299 Cervidae have $\delta^{13}C$ values ranging from -12.89‰ to -9.47‰ (mean = -10.96±0.66‰)
300 and $\delta^{18}O$ values ranging from -8.65‰ to -3.67‰ (mean = -5.96±1.03‰) in the Atlantic sites.
301 These data statistically differ for $\delta^{13}C$ values (Welch t-test: $p = 1.03x10^{-6}$; H_0 = mean are
302 equal), but not for $\delta^{18}O$ values (Welch t-test: $p = 0.71$; H_0 = mean are equal) of Caprinae
303 coming from the same sites (mean $\delta^{13}C$ = -10.12±0.49‰ and mean $\delta^{18}O$ = -6.06±0.88‰).
304 Caprinae from the Atlantic sites have slightly lower $\delta^{13}C$-values (-10.12±0.49‰ against -
305 9.65±0.44‰) and much lower $\delta^{18}O$-values (-6.06±0.88‰ against -1.45±0.74‰), than those
306 originating from Mediterranean sites with $\delta^{13}C$-values of -9.65±0.44‰ and $\delta^{18}O$ -values of -
307 1.45±0.74‰ (Welch t-test for $\delta^{13}C$: $p = 3.6x10^{-3}$; H_0 = mean are equal; Welch t-test for $\delta^{18}O$:
308 $p = 1.7x10^{-16}$; H_0 = mean are equal).
309 Few samples are available for Equidae: 2 samples from Hornos de la Peña and 2 from
310 Laugerie-Haute, have $\delta^{13}C$ and $\delta^{18}O$ values in the range of values from other herbivorous
311 mammals at sites located on the Atlantic side. It is worth pointing out that no temporal trend
312 is observed for either $\delta^{13}C$- or $\delta^{18}O$-values of both Cervidae and Caprinae in the Atlantic sites
313 (Table 1). Nevertheless, whatever their age, Caprinae from this study are characterized by

lower $\delta^{18}O$ values and higher $\delta^{13}C$ values than Cervidae. In addition, statistics that show a normal distribution with relatively small standard deviations are consistent with inter-annual variations of considered climatic parameters.

5. Discussion

5.1. Preservation and meaning of the isotopic compositions

Assessing the potential blurring effect of diagenetic processes represents the greatest challenge for geochemists hoping to reconstruct environmental parameters based on isotopic proxies. Biogenic apatites have undergone diagenesis, at least during the first step of the mineral transformation commonly referred to as "early diagenesis", which follows the decay of the organic matter. Changes in the content of major and trace elements of biogenic apatites do not necessarily mean that their initial stable C- and O-isotope compositions have been fully reset or even partly modified (Goedert et al., 2018). The acquisition of secondary isotopic signatures mainly takes place during the first stages of burial, when processes of mineral dissolution and recrystallization under microbially-mediated conditions may alter the skeletal tissues (Kolodny et al., 1996; Trueman et al., 2003; Zazzo et al., 2004). Enamel is considered a more suitable material for paleoenvironmental or paleoclimatic reconstructions because its apatite carbonate fraction has been shown to be generally resistant to isotopic alteration during early diagenesis due to its highly dense and packed crystallites (Zazzo et al., 2004).

Nonetheless, the preservation of pristine isotopic records needs to be assessed before attempting paleoenvironmental interpretations of the oxygen and carbon isotope compositions of fossil apatites. Whereas there is no method for determining whether the original isotopic compositions are preserved, several tests may help assess the preservation state of the initial isotopic signatures. In the present study, three complementary approaches are used:

i) Although $\delta^{13}C$- and $\delta^{18}O$-values may covariate in the case of specific climate variations, usually detected through geographic or temporal trends (e.g., a combination of higher precipitation and lower temperatures), a linear correlation generally indicates a mixing relationship between two endmembers: the original isotopic signature and a contaminant, such as soil carbonate. Our data do not reveal any such mixing (Atlantic sites {2 outliers}: n = 61; $R^2 = 10^{-3}$; p = 0.76 for H_0: no correlation; Mediterranean sites: n = 13; $R^2 = 3x10^{-2}$; p = 0.57 for H_0: no correlation).

ii) Loose clusters and scrambling of isotopic compositions should affect all tooth material independently of the taxa. Here, the systematic differences in $\delta^{13}C$- and $\delta^{18}O$-values of Cervidae vs Caprinae supports the hypothesis of a preserved isotopic imprint of their respective diets and habitats.

5.2. Reconstitutions of MAP

5.2.1. Method: principles and limits

The $\delta^{13}C$ of consumed food by vertebrates mainly controls the $\delta^{13}C$ of their skeleton (Ambrose, 1993; Ballasse et al., 1999; Szostek, 2009). Carbon isotope ratios of apatite carbonate may be considered as a "dirty window" that opens on a combination of factors: the diet, the degree of openness of the environment (exposure to light) and the amount of precipitation. The reconstruction of MAP is thus done in two steps.

The first step consists in converting the $\delta^{13}C$ of carbonate ($\delta^{13}C_{carb}$) into the $\delta^{13}C$ of diet ($\delta^{13}C_{diet}$), and the second one in converting the $\delta^{13}C_{diet}$ into MAP values ($mm.yr^{-1}$). As a MAP proxy, $\delta^{13}C_{carb}$ is basically tarnished with several important sources of uncertainty. Therefore, we consider that only broad estimates may be obtained. The commonly used isotopic $\delta^{13}C_{carb}$ -$\delta^{13}C_{diet}$ offset value ($\Delta^{13}C_{pl}$) of 14.1‰ (Cerling and Harris, 1999) cannot be used in this study as it varies from one species to another. More recently, Tejada-Lara et al. (2018) proposed a

series of equations that consider the specificities in the digestive system as well as the body mass of different herbivorous mammals. Calculations of $\delta^{13}C_{diet}$ of the study taxa in Table 1 follow this model. It must be kept in mind that animal diets do not necessarily reflect the composition of the vegetation cover; the stricter an animal's food preferences, the larger the bias between the isotopic composition of the diet and that of the vegetation cover.

The second step consists in estimating MAP from the $\delta^{13}C$ of vegetation, here assumed to be close to $\delta^{13}C_{diet}$. The empirical relationship proposed by Rey et al. (2013), which we will use below, is valid if the vegetation cover was composed of C3 plants. This is still an open debate, however, and conflicting reconstructions of the LGM paleovegetation of western Europe from models vs pollen data exist in the literature (e.g., Elenga et al., 2000; Leng, 2006; Woillez et al., 2011; Hatté et al., 2013; Binney et al., 2017; see a discussion and an explanatory hypothesis in Kaplan et al., 2016). Thus, our estimates of MAP from $\delta^{13}C$-data must be seen as a first approximation that needs to be confronted with estimates from other approaches. The method established by Rey et al. (2013), using a least square regression from the dataset of Kohn (2010), is based on relationship (1) below, established between plant leaf discrimination ($\Delta^{13}C_{pl}$) as defined above and mean annual precipitations (MAP):

$$Log_{10}(MAP + 300) = 0.092(\pm 0.004)\Delta^{13}C_{pl} + 1.148(\pm 0.074) \quad (1)$$

with $\Delta^{13}C_{pl} = \frac{\delta^{13}C_{atm} - \delta^{13}C_{pl}}{1 + \frac{\delta^{13}C_{pl}}{1000}}$ and MAP in mm yr^{-1}

$\delta^{13}C_{atm}$ values of atmospheric CO_2 have been measured in air bubbles trapped within the Vostok ice cores between 20 and 43 ka (Leuenberger et al., 1992; Schmitt et al., 2012). For the LGM, this value has been estimated to be close to -7‰ (VPDB). Calculations of MAP are given in Table 1. However, this equation does not consider the pCO_2 effect on $\delta^{13}C$ values of the vegetation (Farquhar et al., 1982; Schubert and Jahren, 2012). Hare et al. (2018) related the $\delta^{13}C$ increase by ≈ 1‰ of plants and faunal collagen to the low pCO_2 values (≈ 180 ppm)

388 of the LGM relatively to those (≈ 300 ppm) of the post deglacial rise that took place about 15
389 kyr ago (Peacock et al., 2006). Consequently, it is most likely that our calculated MAP values
390 according to equation (1) are underestimated by about 150 mm y^{-1}. Final estimates from the
391 model will thus be corrected using this offset.

392 The validity and robustness of this empirical approach were tested successfully in a study
393 (Prud'homme et al., 2018) devoted to the reconstruction of MAP in Germany (Nussloch)
394 during the Last Glacial, which was based on the $\delta^{13}C$ of earthworm granule calcite crystals. In
395 this study, the estimated MAP values range from ~ 270 to 460 mm with a mean value of ~
396 370 mm for the Upper Pleniglacial (~LGM) and of ~ 300 mm, for the Middle Pleniglacial,
397 covering a time interval between 17 ka and 55 ka. Uncertainties associated with the estimated
398 MAP values are on the order of ± 100 to 200 mm. Based on $\delta^{13}C$ values of organic matter
399 preserved in the Nussloch loess deposits and using an inverse modelling approach (BIOME
400 4), Hatté and Guiot (2005) estimated MAP values ranging from 280^{+120}_{-60} to 460^{+80}_{-160} mm.
401 Considering the large uncertainties associated with the various methods of MAP
402 reconstructions, Prud'homme et al. (2018) concluded that the empirical method developed by
403 Kohn (2010) may be used for MAP estimates in the absence of other proxies or modelling
404 approaches.
405
406 5.2.2. Interpretation
407 The reconstructed $\delta^{13}C$-values of animal diet ($\delta^{13}C_{diet}$) suggest that they mainly fed on
408 C3 plants as revealed by a mean $\delta^{13}C_{diet}$ of -23.5±1.0‰ for the whole data base (Table 1),
409 thus supporting the scenario of a C3-plant dominated vegetational cover (compare with Hare
410 et al., 2018). The C3 Calvin-Benson pathway (~75 wt% of the present-day vegetal biomass
411 including trees, temperate grasses, some forbs, shrubs) is the most discriminating regarding
412 the heavy carbon isotopes, thus leading to low $\delta^{13}C$ values ranging from -34‰ to -22‰ and

413 averaging -26‰ (Park and Epstein, 1960; 1961; Smith and Epstein, 1971; O'Leary, 1981).
414 Variations within this range of $\delta^{13}C$ values result from external factors such as air
415 temperature, water stress, exposure to light, $\delta^{13}C$ of atmospheric CO_2, pCO_2 and rate of CO_2
416 recycling (O'Leary, 1981). Worth mentioning is the fact that a $\delta^{13}C_{diet}$ of -23.5±1.0‰ could
417 as well be compatible with a diet of up to ~ 20% of C4 plants, as illustrated for grazers from
418 modern steppe environments (Auerswald et al., 2009). Interestingly, this study also
419 demonstrates that despite a large overall variability of the relative abundance of C4- vs C3-
420 plants, no preferential grazing is observed.

421 Nevertheless, on the Atlantic side of the Iberian Peninsula, Caprinae have higher $\delta^{13}C_{diet}$
422 (mean = -22.8±0.5‰) than Cervidae and Equidae (mean for both = -24.3±0.6‰), all
423 populations being characterized by normal distributions (Caprinae: p = 0.11 and W = 0.953 in
424 the 95% critical range [0.944; 1.000]; Cervidae and Equidae: p = 0.19 and W = 0.960 in the
425 95% critical range [0.942; 1.000]). Such distinct carbon isotope compositions reflect diet
426 differences related to distinct habitats or grazing habits (Figure 2). This observation is in
427 agreement with Jones et al. (2020) who concluded that ibex adapted their niche during the
428 LGM.

429 Among Cervidae, *C. elaphus* have lower $\delta^{13}C_{diet}$ values (mean = -24.4±0.6‰) than *T.*
430 *rangifer* (mean = -23.2±0.36‰), even though only three samples were available of *C.*
431 *elaphus*. A higher $\delta^{13}C_{diet}$ for reindeers, relative to other animals, has been explained by their
432 specific diet mainly based on lichens, especially consumed during the cold season (Park and
433 Epstein, 1960; Máguas and Brugnoli, 1996; Ben-David et al., 2001)

434 Based on the estimated $\delta^{13}C_{diet}$ values, MAP values were calculated in the range ~ 100 to
435 400 $mm.yr^{-1}$ for Atlantic sites (100 to 200 $mm.yr^{-1}$ recorded by Caprinae and 200 to 400

436 mm.yr^{-1} recorded by Cervidae and Equidae), while they are close to 100 mm.yr^{-1} for the two
437 Mediterranean sites (Table 2). The present-day reference values (Table 2) extracted from
438 meteorological records (IAEA/WMO database) correspond to cities in the vicinity of the
439 studied archaeological sites, specifically Almeria (202±66 mm.yr^{-1}), for the Nerja site,
440 Valencia (532±173 mm.yr^{-1}), for the Malladetes site , Santader (1050±140 mm.yr^{-1}), for the
441 sites located in Asturias and Cantabria (Spain), and Cestas-Pierroton (937±192 mm.yr^{-1}), for
442 the Laugerie-Haute site. The Caprinae record of drier environmental conditions than those
443 inferred from Cervidae and Equidae, suggests differences in diets and/or seasonal/altitudinal
444 grazing habitats between some of the representative herbivorous species sampled.

445 Diet preferences between C3 and C4 may cause $\delta^{13}C$ differences by several ‰ between
446 sheep and goat, for example, as shown by Balasse and Ambrose (2005) for C4 grassland
447 environments of the Central Rift Valley of Kenya. However, C4 was most likely absent or
448 very scarce in the studied LGM-environments (Collins and Jones, 1985). $\delta^{13}C$ differences
449 among C3-eating large mammals may result from differences in water stress and/or exposure
450 to light (O'Leary, 1981). It means that $\delta^{13}C$ values of Caprinae should be higher than those of
451 Cervidae and Equidae if the Caprinae habitat was open (sparse vegetation cover in a rocky
452 environment) and characterized by a vegetation submitted to water stress (e.g. dry sides of
453 mountains).

454 Nevertheless, during the LGM, precipitation followed a pattern similar to the modern one
455 (Figure 3), with sites under Atlantic vs Mediterranean influence defining two distinct clusters.
456 The Mediterranean cluster is significantly drier than the Atlantic one, but both depict much
457 drier conditions than at present. LGM precipitation estimates obtained here broadly agree
458 with pollen-based reconstructions (e.g., Peyron et al., 1998), but disagree with the wetter
459 conditions reconstructed from climate model experiments (e.g., Ludwig et al., 2016; Arpe et
460 al., 2011).

461

462 5.3. Reconstitutions of MAAT

463 5.3.1. Method: principles and limits

464 Oxygen isotope ratios of apatite carbonate may be seen as a “frosted glass window” open
465 on the composition of dietary sources of water and local meteoric water, ultimately used as a
466 proxy for air temperatures (e.g. Fricke and O’Neil, 1998; Daux et al., 2005). The $\delta^{18}O$ of
467 consumed water by vertebrates mainly controls the $\delta^{18}O_c$ of their skeleton (Longinelli, 1984;
468 Kohn, 1996). The oxygen isotope composition of leaf water can somewhat blur the
469 relationship between the $\delta^{18}O_c$ of apatite carbonate and the $\delta^{18}O$ of drinking water (Ayliffe
470 and Chivas, 1990; Cormie et al., 1994; Luz et al., 1990; Pederzani and Britton, 2019). It
471 constitutes, however, a good indicator of aridity (Levin et al., 2016; Blumenthal et al., 2017).

472 In this approach, the reconstitution of MAAT is done in four steps.

473 First, oxygen isotope compositions of apatite carbonate ($\delta^{18}O_c$) measured on the VPDB
474 scale (Coplen et al., 1983) must be converted into those of their phosphate counterparts
475 ($\delta^{18}O_p$) before being used to estimate the composition of drinking water on the basis of the
476 equations available in the literature. This step is achieved by using equation (2) that was
477 determined by Iacumin et al. (1996) for modern herbivorous mammals. Unfortunately, this
478 step is a source of large uncertainties ($\delta^{18}O_p$: standard error of estimate = 0.73). We computed
479 Equation (2) using the original data set published in Iacumin et al. (1996) in order to tighten
480 uncertainties as follows:

481 $$\delta^{18}O_p = 0.975(\pm0.031)\ \delta^{18}O_c - 8.43(\pm0.81) \quad (n = 17;\ R^2 = 0.985) \qquad (2)$$

482 The second step consists in calculating the oxygen isotope composition of water
483 consumed (free water and water derived from the food such as leaves and herbs) by the
484 animals. Several oxygen isotope fractionation equations between apatite phosphate ($\delta^{18}O_p$)
485 and water ($\delta^{18}O_w$) have been published for large herbivorous mammals, covering all taxa

investigated in the present study. It is worthy to note that animal physiology is integrated in the oxygen isotope fractionation equations (Longinelli, 1984; Luz and Kolodny, 1985; Kohn, 1996; Langlois et al., 2003) that have been established on present-day fauna, either the same species or close relatives. The relevant equations have also been recalculated to set the $\delta^{18}O_w$ variable as the estimator (Y-axis) in the regression line along with the associated statistics, as follows:

- Deer (*Cervus elaphus*) (D'Angella and Longinelli, 1990):

$$\delta^{18}O_w = 0.88(\pm0.03)\delta^{18}O_p - 22.50(\pm0.52) \quad (n = 7; R^2 = 0.99) \quad (3)$$

- Reindeer (*Rangifer tarandus*) (Iacumin and Longinelli, 2002):

$$\delta^{18}O_w = 1.21(\pm0.01)\delta^{18}O_p - 26.41(\pm1.31) \quad (n = 34; R^2 = 0.74) \quad (4)$$

Note that 2 outliers were removed from the original database for the setting of equation 4, as recommended by Iacumin and Longinelli (2002).

- Horse (*Equus burchelli, E. zebra, E. caballus*) (Bryant et al., 1994; Sanchez Chillon et al., 1994; Delgado-Huertas et al., 1995):

$$\delta^{18}O_w = 1.09(\pm0.128)\delta^{18}O_p - 25.83(\pm1.08) \quad (n = 25; R^2 = 0.77) \quad (5)$$

Note again that 2 outliers were removed from the original database deduced from linear regression analysis

- Wild Goat (*Capra hircus and C. ibex*) (Delgado-Huertas et al., 1995)

$$\delta^{18}O_w = 1.09(\pm0.06)\delta^{18}O_p - 26.45(\pm0.98) \quad (n = 21; R^2 = 0.95) \quad (6)$$

A major caveat here is the possibility of distinct $\delta^{18}O_w$ vs $\delta^{18}O_p$ relationships during the cold LGM, due to reduced evapotranspiration (e.g., Kohn, 1996). Isotope enrichment from precipitation to plant-water and finally to the animal body-water could have prevailed. Thus, under LGM conditions, the $\delta^{18}O_w$-value calculated with the above equations must be seen as a maximum value.

510 The third step consists in correcting the $\delta^{18}O$ of seawater from the volume of
511 continental ice. Indeed, any change in the isotopic composition of oceanic sources will
512 propagate throughout the entire surface water cycle. Knowing that the mean depth of the
513 oceans is 3,700 m (Charette and Smith, 2010), a decrease in sea level by 120±10 m (Lambeck
514 et al., 2014) results in a mean increase of the global ocean reservoir $\delta^{18}O$-value by +1.2±0.1‰
515 provided the mean $\delta^{18}O$ of the LGM ice-sheets is close to -40‰ (Blunier and Brook, 2001).
516 This isotopic offset is very close to that proposed by Schrag et al. (2002) and Steele et al.
517 (2009), but perhaps a little overestimated, based on isotopic composition for the Laurentide
518 Ice Sheet proposed by Hillaire-Marcel and Causse (1989) or Sima et al. (2006). Duplessy et
519 al. (2002) proposed an offset of 1.05±0.20‰ probably encompassing the effective overall
520 change in the ocean isotopic composition. However, moisture sources relate to ocean surface
521 water masses: their isotopic composition differs from that of the whole ocean, and may show
522 large regional offsets, especially in the present case, between the Bay of Biscay and the
523 western Mediterranean. The Bay of Biscay was likely the major moisture supplier for the
524 Atlantic sites, whereas a mixture of Atlantic and western Mediterranean moisture supplies
525 may be hypothesized for the Mediterranean sites. The two marine areas were of course
526 characterized by distinct MAAT, mean salinity and isotopic composition.
527 Based on Schrag et al. (2002), one may assume an isotopic composition of surface
528 waters from the northeast North Atlantic in the +0.7±0.1 to +0.8±0.1‰ range vs VSMOW, a
529 range compatible with model estimates from Paul et al. (2001). According to Loncaric et al.
530 (1998), MAAT depicted large amplitude oscillations between <5°C and up to 15°C, with a
531 mean value of about 7 to 9°C (e.g., Kuhlemann et al., 2008). Comparatively, surface waters
532 from the western Mediterranean were not only warmer but enriched in ^{18}O. Planktic
533 foraminifera (Hayes et al., 2005) and biomarkers (Rodrigo-Gámiz et al., 2014), both
534 suggesting a mean LGM sea-surface temperature (SST) of ~ 13.5°C, whereas $\delta^{18}O_{carb}$ values

535 reported from this sector of the Mediterranean during the same interval range from
536 +3.5±0.5‰ vs VPDB in planktic foraminifera (Thunell and Williams, 1989) to +3.9±0.2 ‰ in
537 shallow mollusk shells (Fergusson et al., 2011). Combining these values, one may set the
538 LGM $\delta^{18}O_{sw}$-value at about +3‰ vs VSMOW in the western Mediterranean, to be compared
539 with a modern value of ~ +1.3‰ (Goddard Institute data base; Schmidt et al., 1999; see also
540 Benetti et al., 2017). Potential moisture generated during the evaporation of the western
541 Mediterranean Sea, which had a $\delta^{18}O$ higher than the Atlantic Ocean by ~ +2‰, may thus
542 have played some role during the LGM. However, climate models suggest a southward shift
543 of the North Atlantic jet stream during the LGM, governing the relatively abundant winter
544 precipitation in comparison with summer rains which were somewhat controlled by local
545 processes (e.g., Beghin et al., 2016). Thus, the most likely LGM moisture source, for both the
546 Mediterranean and the Atlantic sites, would have been the northeastern North Atlantic Ocean,
547 leading to adopt the $\delta^{18}O_{sw}$ ~ +0.8‰ value for the primary source water, and allowing for
548 some ^{18}O-enriched precipitation in summer, influenced by the high $\delta^{18}O_{sw}$-values of the
549 western Mediterranean waters (~ + 3‰). Perhaps worth of mention here is the fact that under
550 the modern conditions, i.e., with a $\Delta\delta^{18}O$ offset of ~ +0.8‰ between surface waters of the
551 western Mediterranean ($\delta^{18}O_{sw}$ ~ 1.3‰) and those of the northeastern North Atlantic ($\delta^{18}O_{sw}$
552 ~ 0.5‰; Benetti et al., 2017), the long-term isotopic composition of precipitation in both areas
553 is almost similar (~ -6‰; Araguas-Araguas et al., 2005), thus pointing even today to a major
554 contribution of Atlantic moisture sources to precipitation on the Iberian Peninsula.
555 We used the +0.8‰ offset between modern vs LGM moisture sources as a base line
556 for both regions and subtracted it from the $\delta^{18}O_w$-values derived from equations (3) to (6) (see
557 Table 1). Nevertheless, we also increased this offset to +1.2‰ for the Mediterranean sites, a
558 value that would account for about 20% of Mediterranean moisture source supplies on a
559 yearly basis, based on the ~ 2‰ offset in $\delta^{18}O_{sw}$-values between the Bay of Biscay and the

560 Western Mediterranean. Again, this seems a reasonable estimate considering the regional
561 atmospheric circulation in SW Europe during the LGM (cf. Ludwig et al., 2016; see also
562 Kuhlemann et al., 2008; Beghin et al., 2016).

563 The fourth step aims at converting $\delta^{18}O_w$ to MAAT. Here again, one may question
564 whether or not present-day relationships fully apply to the LGM. Firstly, all of the sites of the
565 present study are close to coastlines, thus, they are not affected by continental Rayleigh-
566 evolution of humid air-masses or by major altitudinal effects (e.g., Gat et al., 2001), a process
567 well illustrated by Rozanski et al. (1982) for inland precipitation patterns in Europe. Isotopic
568 compositions of precipitation at the study sites should then follow a relatively linear
569 relationship with mean annual temperatures, as observed at global scale, despite some
570 latitudinal/regional variations in the slope and intercept of the local regression lines (e.g., Lee
571 et al., 2008). The slope of a MAT–$\delta^{18}O_{mw}$ linear relationship is mainly temperature–
572 dependent at mid- and high-latitudes. This point is firstly well illustrated by the existence of a
573 strongly positive linear correlation (R^2 = 0.83) between the dew point (T_d) and the oxygen
574 isotope composition of meteoric water (Figure 4). T_d, expressed in °C, represents the
575 temperature at which the actual water vapour pressure equals the saturated water vapour
576 pressure (RH = 100%). This climatic parameter plays a key role in the distribution of $\delta^{18}O_{mw}$
577 over the continental masses located in the mid-latitudes (Lécuyer et al., 2020). Secondly,
578 there is a unique MAT–$\delta^{18}O_{mw}$ linear relationship for present-day (Figure 5A) for latitudes >
579 32°, even if it samples various continental areas from both hemispheres, which are submitted
580 to various moisture-bearing prevailing winds.

581 The MAAT (in °C) vs $\delta^{18}O_w$ linear relationship from equation (7), established for
582 Europe (Skrzypek et al., 2011), is indistinguishable in terms of slope and intercept from
583 equation (8) obtained at a global scale (Figure 5A). For a reliable comparison, equation (8)

584 was computed by excluding data from the tropics as well as those corresponding to air
585 temperatures lower than 0°C (Figure 5B).

586 $$MAAT\ (°C) = 1.41\ \delta^{18}O_{w\text{-}MAP} + 21.63 \quad (7)$$

587 where MAT represents the mean annual temperature and $\delta^{18}O_{w\text{-}MAP}$, the weighted mean
588 isotopic composition of annual precipitation.

589 $$MAAT\ (°C) = 1.40(\pm0.08)\ \delta^{18}O_{w\text{-}MAP} + 21.86(\pm0.64) \quad (8)$$

590 $$(n = 90;\ R^2 = 0.81)$$

591 Equation (7) was thus used to calculate MAAT (reported in Table 1) during the LGM in
592 southwestern Europe. There are three caveats when using this method:

593 1) Altitude effect: in Spain, the rate of air-temperature decrease with altitude is close to 5°C
594 per 1000 m in mountain areas (Navarro-Serrano et al., 2018). In the Pyrenees, altitudinal
595 oxygen isotope gradients average -3‰ per 1000 m (Hughes et al., 2018), a value within
596 the range observed in southern Europe (e.g., Tazioli et al., 2019). Consequently,
597 differences between present-day reference stations (cities are close to sea-level) and
598 mammal ranges (between 0 and 1000 m) during the LGM may lead to overestimates of
599 temperature differences by about 2°C in northern Spain and up to 4°C in south and
600 southeast Spain.

601 2) Source effect: the source of drinking water may differ isotopically from local meteoric
602 waters, for example in rivers since their sources are located at altitudes. A comparison
603 between present-day river and precipitation $\delta^{18}O$ maps (Nan et al., 2019) reveals that
604 differences between those two parameters are close to 2‰ over Europe on a yearly
605 average. Once again, true air temperatures may be higher than those calculated following
606 the above method. Similarly, animals that seasonally migrate may have a $\delta^{18}O_w$ record
607 that is biased relative to their place of death.

3) Reservoir effect: water stored in ponds, lakes or in snow cover may suffer evaporation or sublimation that tends to enrich the residual liquid–solid water in heavy isotopes. Such processes may induce oxygen isotope biases in the order of a few per mil.

However, a sporadic influence of the above boundary conditions on the isotopic approach should be detectable by altering the normal distribution of the studied population; which does not seem to be the case here.

5.3.2. Interpretation

$\delta^{18}O_{w\text{-}MAP}$ have been calculated according either to ocean surface water having a $\delta^{18}O$ of +1.2 or +0.8‰. Inferred temperatures using equation (7) are shifted by ≈ +0.6°C. In the case of a prevailing oceanic surface source of moisture having a $\delta^{18}O$ of +1.2‰, calculated mean $\delta^{18}O_{w\text{-}MAP}$ are -10.1±0.9‰ (n = 46) and -10.3±1.0‰ (n = 17) for northern Spain and Laugerie-Haute, respectively (Table 1). Pooled data follow a normal distribution (Figure 6) according to the Shapiro-Wilk test (p = 0.26 and W = 0.976 in the 95% critical range [0.9620; 1.000]). The range of $\delta^{18}O_{w\text{-}MAP}$ values comprised between ~ -12‰ and ~ -8‰ correspond to present-day compositions of precipitation in south Scandinavia and Central Europe (IAEA/WMO database and maps). Calculated mean $\delta^{18}O_{w\text{-}MAP}$ are -5.4±0.8‰ (n = 8) and -5.8±0.8‰ (n = 6) for Malladetes and Nerja, respectively. Pooled data follow a normal distribution (Figure 6) according to the Shapiro-Wilk test (p = 0.93 and W = 0.975 in the 95% critical range [0.875; 1.000]). The range of $\delta^{18}O_{mw}$ values between ~ -7‰ and ~ -4‰ correspond to present-day compositions of precipitation along the Mediterranean rim (IAEA/WMO database and maps).

The calculated $\delta^{18}O_{w\text{-}MAP}$ values based on a $\delta^{18}O_{sw}$ of +0.8‰ range from ~ 6°C to ~ 10°C for Atlantic sites. This range may be explained by altitudinal gradients recorded by the faunal remains and/or by the large amplitude oscillations of LGM-SST and LGM-$\delta^{18}O_{carb}$

values in the Bay of Biscay reported by Loncaric et al. (1998). It is interesting that the range of temperature inferred for the Atlantic sites in the present study is within the range proposed by these authors for surface waters of the Bay of Biscay during the LGM. On the Mediterranean side, the estimated LGM-MAAT values are close to 14–15°C for both sites ($\delta^{18}O_{sw}$ of +0.8‰) or close to 13.5–14.5°C ($\delta^{18}O_{sw}$ of +1.2‰) when accounting for some contribution of Mediterranean moisture to summer precipitations (Table 2). Here also, this value is practically identical to LGM-SST values in the Western Mediterranean estimated by Hayes et al. (2005) or by Rodrigo-Gámiz et al., (2014).

The air temperatures reconstructed during the LGM are lower than the present-day ranges recorded in meteorological stations located either in the vicinity of the Atlantic sites (Santander: 14.8±0.4°C and Cestas-Pierroton: 13.1±0.6°C), or close to the Mediterranean sites (Almeria: 19.2±0.4°C; Valencia: 18.5±0.6°C). As shown in Figure 7, MAAT decreased during the LGM from South to North according to a trend roughly similar to the modern one. As a whole, MAAT values in southern Spain were about 4–5°C below modern pre-industrial temperatures, and by 5–8°C in northern Spain and southwest France (Figure 7).

5.4. LGM climate inferred from large mammal isotopes and biogeographic patterns.

Faunal associations described in the archaeological sites of southwestern Europe are generally compatible with cold and dry, open environments, such as tundra and dry steppe, but there are important regional differences. The sites sampled in this study are from three distinct biogeographic zones, following the classification suggested by Yravedra and Brugal (2005) for southwestern Europe. The zones sampled for this study are: southwest France (zone VI), Cantabria/Asturias (zone IV) and the Mediterranean coast (zone IIIa). A general reduction in faunal diversity is observable in Southwestern Europe during the LGM, signaling the severity of the climate downturn, but the relative diversity of herbivores and carnivores

658 differs between zones. Diversity decreases in zone VI reaching minimum levels during the
659 LGM, in zone IV (Cantabria/Asturias) diversity also decreases but reaches a minimum after
660 the LGM, while carnivore diversity actually increases with time, whereas the opposite pattern
661 occurs in zone IIIa (e.g., Valencia) where a gradual increase in herbivore diversity is
662 observable over the course of the last Glacial (Yravedra and Brugal, 2005).

663 In SW France (zone VI), horse dominates sites such as Laugerie Haute Est at the
664 beginning of the LGM (e.g., in the Magdalenian 0 level; Table 1) but reindeer, a taxon
665 associated with tundra environments, increases dramatically in importance throughout the
666 sequence, eventually dominating during Magdalenian I and II (see: Delpech, 2012). In
667 northwest Spain (zone IV), on the other hand red deer, a taxon generally considered more
668 indicative of temperate, wooded contexts often dominates late Glacial faunal assemblages,
669 while the proximity of sites to the coastal ranges is signaled by the presence of ibex and
670 chamois (Straus, 2018). Our results are consistent with the biogeographic patterns described
671 above, indicating strong contrasts between Mediterranean sites (in Zone IIIa) and sites in
672 zones IV and VI in terms of MAAT and MAP.

673 During the LGM, tundra extended across northern Europe while steppes dominated
674 the Mediterranean areas, resulting in a geographic reduction and fragmentation of boreal
675 evergreen forests (taiga) and temperate deciduous forests (Tarasov et al., 2000). The mean
676 value of 350±100 mm.yr^{-1} reconstructed for MAP from the $\delta^{13}C_{carb}$ of the dental apatite of
677 herbivorous mammals (above) is consistent with this observation. However, a few samples of
678 *Cervus elaphus* from zone IV, El Cierro and El Ruso, the closest to the Atlantic ocean depict
679 a $\delta^{13}C_{carb}$-value low enough to suggest that some years or periods in the year were
680 characterized by MAP $\geq$ 500 mm.yr^{-1}. This could mean that the climate in northern Spain was
681 rather unstable at inter-decadal or inter-centennial scales towards the end of the LGM, or

682 simply that *C. elaphus* used a large seasonal altitudinal range, as observed in modern
683 specimens in the Alps (Luccarini et al., 2006) or from the Rockies (Morgantini et al., 1989).
684 Geochemical proxies similar to those used in this study were applied to faunal remains
685 (horse, deer and ibex) recovered from the archaeological site of Peña Capón (Yravedra et al.,
686 2016), a rock shelter located in central Iberia which contains sedimentary deposits assigned to
687 Marine Isotope Stage 2 (MIS 2). Yravedra et al. (2016) estimated MAAT for archaeological
688 levels with a ^{14}C cal. age of ~23.8 kyr, ranging from 9°C to 12°C, i.e. only slightly below the
689 present-day MAAT of 12°C–13°C recorded in the locality of Muriel. These estimates for the
690 central part of the Iberian Peninsula may reflect milder conditions prior to the onset of the
691 LGM. Nevertheless, it is interesting to note that they are bracketed by our results. It is also
692 worthy to note that ibex recorded higher $\delta^{13}C$ values and lower $\delta^{18}O$ values than the other co-
693 habitating mammals such as Cervidae and Equidae. These data point to a specific habitat for
694 Caprinae as recently suggested by Jones et al. (2020) who analyzed both carbon and nitrogen
695 isotope compositions of bone collagen. These authors concluded that the existence of refugia
696 in south Europe allowed most herbivores to adapt despite harsh and fluctuating climatic
697 conditions.
698 The LGM climate conditions have been reconstructed from palynological data (e.g.,
699 Peyron et al., 1998). In the north of Spain (Lago Ajo) and in the south (Padul), MAAT values
700 were estimated in the 10°C to 5°C range. Palynological estimates of MAP, range from 900-
701 600 mm in the north of Spain, to close to 200 mm in the south. The temperatures from
702 palynological records are congruent with the estimates of the present study. However,
703 whereas paleoprecipitation estimates from palynology or from the present isotopic approach
704 fit well in zone IIIa, on the Mediterranean side, the MAP estimates for Northern Spain from
705 pollen proxies are somewhat higher than those based on $\delta^{13}C_{carb}$ values. This leads us to
706 consider the possibility that isotopic reconstructions, such as used here, vs reconstructions

707 from transfer function using palynological assemblages, do not necessarily encompass the
708 same space-time dimensions. For example, differences in the seasonality of pollen production
709 and patterns of altitudinal grazing may result in distinct signals.

710 As mentioned above, the study sites are close to either the Bay of Biscay (in zones IV
711 and VI) or the western Mediterranean (zone IIIa). Hayes et al. (2005) and Rodrigo-Gámiz et
712 al. (2014) estimated LGM-SSTs of ~ 13.5°C off the Mediterranean coastline of Spain,
713 whereas Kucera et al. (2005) estimated LGM-SST of ~ 8°C for the Bay of Biscay on the basis
714 of foraminifera $\delta^{18}O$ values. Both values fit with the corresponding inland, but coastal
715 temperatures reconstructed here, highlighting the strong influence of adjacent marine basin
716 SSTs on proximal inland MAAT. Moreover, these temperature estimates based on marine as
717 well as on continental proxies, enforce the hypothesis of cold regional conditions as well as of
718 a marked difference between the Atlantic and Mediterranean zones; the latter being less
719 affected by global LGM cooling.

720 At odds with these results are the model outputs of paleo-glaciers (Allen et al., 2008),
721 which provided both large amounts of precipitation (1000 to 1400 $mm.yr^{-1}$) and temperature
722 anomalies from -16°C to -11°C in northern and southern Spain, respectively. Such climatic
723 patterns cannot be easily reconciled with the present knowledge of the LGM vegetation cover
724 and faunal associations (Sommer and Nadachowski, 2006; Benito Garzón et al., 2007;
725 Morales-Molino and García-Antón, 2014; Binney et al., 2017; Quinzin et al., 2017).

726 Atmosphere-ocean global climate models (GCMs) computed global mean LGM-air
727 temperatures 4°C to 7°C lower than Present, when adding feedback effects due to changes in
728 the vegetation cover and the amount of atmospheric dust (Crucifix and Hewitt, 2005; Jansen
729 et al., 2007; Roche et al., 2007; Cao et al., 2019). In southwest Europe, the air temperature
730 anomaly was estimated between -8°C and -4°C based on a multi-model regression of proxy
731 data and PMIP2 model output (Annan and Hargreaves, 2013). Mean annual air temperatures

anomalies were also estimated in the range -10°C to -5°C for ice-free areas of Europe, based on a regional climate model (Strandberg et al., 2011). Jost et al. (2005) emphasized the need of high-resolution spatial climate models to solve discrepancies with reconstructions based on proxies such as pollen assemblages. Models tend to underestimate the magnitude of cooling (especially in winter) with the consequence of overestimating the amount of precipitation. When applied to Europe, most simulated climates, such as the those of the *Paleoclimate Modelling Intercomparison Project* (PMIP) or from refined General Climate Model (GCM), generate warmer and wetter LGM-conditions than those inferred from palynological or geochemical proxies (Kageyama et al., 2001; Latombe et al. 2018; present study). Latombe et al. (2018) study indicates temperatures and precipitation were close to 5-6°C and 200-250 mm y^{-1} in northern Spain, close to 7°C and 160 mm y^{-1} at Laugerie-Haute, and close to 11°C and 225 mm y^{-1} at Nerja, in southern Spain. Within uncertainties, such air temperatures are coherent with those estimated from our isotopic proxy approach even though Latombe et al. (2018) obtained slightly lower temperatures for Nerja. Our MAP estimates are generally slightly higher than those modeled by Latombe et al. (2018), especially in the case of northern Spain.

Spatial resolution is critical in areas either close to the ocean (e.g., Atlantic Ocean) or along a mountain range (e.g., Pyrenees). Kageyama et al. (2006) performed a comparison of PMIP models, SSTs from MARGO (*Multiproxy Approach for the Reconstruction of the Glacial Ocean surface*) and pollen-based reconstructions over Europe. These authors highlighted the main data-model discrepancy observed for western Europe, with winter temperatures underestimated by all models that could be at least partly explained by a high interannual variability in the temperatures of the coldest months. However, more recent high-resolution climatic simulations tend to reduce the discrepancy vs geochemical proxy-derived temperature estimates. This is for example the case of the central part of Iberia (~ 21 ka) with

757 a computed MAAT close to 7±3°C (Burke et al., 2014) that are comparable or only slightly
758 higher than those inferred from the oxygen isotope composition of large mammals (Yravedra
759 et al., 2016).

760 The geochemical data presented in our study do not provide a temporal resolution at
761 the seasonal scale, but large inter-annual variations in winter air temperatures should be
762 imprinted on the half-year or full year time record provided by mammal tooth enamel. For the
763 studied archaeological sites located on the Atlantic side, the range of $\delta^{18}O_{w\text{-}MAP}$ is 4‰ (Figure
764 6), which corresponds to a temperature variation of ±5.5°C around the mean, according to
765 equation (7). If interpreted as inter-decadal or inter-centennial variations in MAAT, such a
766 magnitude is higher than that observed (2±1°C) during periods of relative climate steadiness
767 (e.g., Corona et al., 2010; Ljungqvist et al., 2019). Whether this temperature variation of
768 ±5.5°C indicates high-frequency climate instabilities in western Europe during the LGM, in
769 agreement with Jones et al. (2020)'s or Loncaric et al. (1998), remains to be further
770 investigated.

771 Climate conditions on the Iberian Peninsula are driven by large-scale processes that
772 create strong regional contrasts in rainfall and temperature values. Our results demonstrate
773 that these contrasts are reliably recorded in hard tissues and that isotope analyses of vertebrate
774 remains can be used as proxies of mean annual temperature and precipitations on a regional
775 scale. We confirm that, during the LGM, populations living in Franco-Cantabria and on the
776 Mediterranean coast faced different environmental challenges. As the paleontological and
777 archaeozoological records demonstrate it (Brugal and Yravedra, 2005) this difference
778 impacted the relative availability of different prey species, which would have required
779 adjustments of human hunting strategies, potentially driving technological change. Indeed, the
780 LGM coincides with the appearance of the Solutrean technocomplex, which is geographically
781 limited to the Iberian Peninsula and France. Three Solutrean "culture areas" (Andalucia,

782 Portugal and Vasco-Cantabria) are described for the Iberian Peninsula (Straus, 2000) and
783 these differences in the material culture used by human groups could reflect regional
784 adaptations to contrasting environmental conditions such as those described here. These
785 results are also consistent with archaeological research using an agent-based model that
786 suggests that the population of Western Europe was spatially fragmented during the LGM as
787 a result of climate-driven differences in habitat suitability (Wren and Burke, 2018). In this
788 latter study, the SE region of the Iberian Peninsula was described as a "sink" during the LGM,
789 with human population numbers declining periodically and being replenished from a larger
790 "source" population, located in SE France and NE Spain.

791 Considering the uncertainties associated with our stable isotope proxy approach,
792 including the altitudinal effect that is not easy to constrain, the present MAAT estimates are
793 coherent with those inferred from other proxies (pollens, foraminifera) and some recent model
794 outputs. In the case of MAP reconstructions, the isotopic approach suggests dry environments
795 in agreement with our knowledge of LGM-flora and faunal associations. However, most
796 modeling approaches still generate divergent patterns with some of them suggesting
797 paleoenvironments as wet as those of today, or even more, along with similar MAAT.

798 Future research priorities may focus on the initial conditions required by the GCM
799 models to reproduce the dry and cold conditions of the LGM in southwestern Europe. In
800 addition, reconstructing the amplitude of precipitation and air temperature seasonality by
801 high-resolution incremental sampling of tooth enamel may be of great interest. Indeed,
802 mammals could have fed on resources (water, vegetation) mainly renewed during the winter
803 and intermediate seasons, not in summer, hence biasing the isotopic record at least toward too
804 negative mean air temperatures.

805

806 ## 6. Conclusions

Our study documents the carbon and oxygen isotope composition of tooth enamel carbonate of Cervidae, Equidae and Caprinae remains dated to the LGM in southwest Europe. The $\delta^{13}C$ of tooth enamel carbonate was ultimately used to obtain semi-quantitative estimates of MAP. Precipitation in the range of ~ 250 to 550 $mm.yr^{-1}$ were obtained for Atlantic sites and values close to 250 $mm.yr^{-1}$ for the Mediterranean sites; both estimates are lower than local precipitation today (200–1000 $mm.yr^{-1}$). Despite the large uncertainties associated with each step of the method, the reconstruction of a dry and cold LGM environment is consistent with the faunal and floral associations documented for this period. The limitation of the $\delta^{13}C$ method for estimating paleo-precipitation is mainly related to the behavior of the studied vertebrate species. The observed $\delta^{13}C$ differences between Caprinae and Cervidae or Equidae, for example, most likely reflects habitat use, with Caprinae occupying possibly drier habitats.

The $\delta^{18}O$ of tooth enamel carbonate was used for estimating MAAT. In southern Spain, temperatures during the LGM were lower by about 4–5°C relative to modern times and lower by 5–8°C in northern Spain and southwest France. Several steps are necessary to calculate MAAT, and each one potentially propagates sizable uncertainties due to the combined use of empirical linear equations relating the isotopic compositions of the biomineral, the meteoric water and the air temperature. Moreover, we identified additional sources of uncertainties. The first two are related to an "altitude effect" and a "source effect" that lead to an overestimate of the air temperature differences between the LGM and the present day on the order of a few °C. The third one, which we refer to as the "reservoir effect", relates to the ^{18}O-enrichment of meteoric waters stored in a natural reservoir (pond, lake, snow cover) open to the atmosphere and subsequently exposed to evaporation. In this case, the lower the residence time of water in the reservoir, the higher the increase in the $\delta^{18}O$ of stored water, hence leading to a potential overestimation of air temperatures.

At first glance, our estimates of MAP and MAAT are compatible with the faunal associations described in the archaeological sites of southwestern Europe with generally cold and dry, open environments such as tundra and dry steppe. Sea surface temperatures inferred from the oxygen isotope composition of planktonic foraminifera enforce the hypothesis of cold regional conditions as well as a marked difference between the Atlantic and Mediterranean sides; the latter being less impacted by the global cooling.

Close to montane areas, topography is highly variable with a juxtaposition of micro-climates that makes a comparison of geochemical proxy results with model outputs risky and potentially fruitless, considering the unresolved differences in temporal and spatial resolution inherent in both scientific approaches. Nevertheless, there is room for improvement with, for example, the reconstitution of the seasonal amplitude of precipitation and air temperature performed by high-resolution incremental sampling of vertebrate tooth enamel. Precipitation and air temperature for the coldest and warmest months could be directly compared to model output with the aim to identify potential biases intrinsic to each method.

Acknowledgements – We are grateful to A. Álvarez-Fernández and J. Bécares (Universidad de Salamanca), E. Aura Tortosa and E. Muñoz Fernández (Colectivo para la Ampliación de Estudios de Arqueología Prehistórica), C. Cacho (Museo Arqueológico Nacional), A. Chauvin and R. Ontañón (Museo de Prehistoria y Arqueología de Cantabria), J-J. Cleyet-Merle and S. Madeleine (Musée national de Préhistoire), M. Pérez Ripoll (Universitat de València) and J. Yravedra (Complutense University) for their great and kind help during the first stages of this study, as well as for providing access to samples and allowing us to work in their different laboratories. We warmly thank J. Lepage for her help in the data collection, who was awarded an MEESR mobility grant. This study was possible thanks to an Early Career Research grant to MAJ. This research was supported by the Fonds de Recherche du

856 Québec Société et Culture, grant #SE-179537 (to AB). A NSERC-Canada Discovery Grant to
857 chm and an infrastructure award from the Fonds de Recherche du Québec en Sciences
858 Naturelles et Technologie to Geotop supported the analytical work. Three anonymous
859 reviewers are thanked for their comments and suggestions that helped to improve our
860 interpretations.

861
862

References

Allen, R., Siegert, M. J., Payne, A. J., 2008. Reconstructing glacier-based climates of LGM Europe and Russia–Part 2: A dataset of LGM precipitation/temperature relations derived from degree-day modelling of palaeo glaciers. Climate of the Past, 4(4), 249-263.

Álvarez-Fernández, E., Álvarez-Alonso, D., Bécares, J., Carral, P., Carriol, R.-P., Chauvin, A., Cubas, M., Cueto, M., Domingo, R., Douka, K., Emorza, M., Jordá-Pardo, J.F., Murelaga, X., Portero, R., Rivero, O., Tapia, J., Tarriño, A., Teira, L.C., 2016. Nouvelles données sur le Magdalénien inférieur de la Région Cantabrique: le Niveau F de la grotte de El Cierro (Ribadesella, Asturies, Espagne). L'Anthropologie 120, 537–567.

Álvarez-Lao, D. J., and García, N., 2011a. Southern dispersal and Palaeoecological implications of woolly rhinoceros (*Coelodonta antiquitatis*): review of the Iberian occurrences. Quaternary Science Reviews 30, 2002–2017.

Álvarez-Lao, D. J., and García, N., 2011b. Geographical distribution of Pleistocene cold-adapted large mammal faunas in the Iberian Peninsula. Quaternary International 233, 159–170.

Ambrose, S. H., and Norr, L., 1993. Experimental evidence for the relationship of the carbon isotope ratios of whole diet and dietary protein to those of bone collagen and carbonate. In Prehistoric human bone (pp. 1-37). Springer, Berlin, Heidelberg.

Annan, J. D., and Hargreaves, J. C., 2013. A new global reconstruction of temperature changes at the Last Glacial Maximum. Climate of the Past 9, 367–376.

Araguas-Araguas, L. J., Diaz Teijeiro, M. F., 2005. Isotope composition of precipitation and water vapour in the Iberian Peninsula: first results of the Spanish network of isotopes in precipitation. International Atomic Energy Agency Technical Report 1453, 173–190.

Arpe, K., Leroy, S.A.G., Mikolajewicz, K., 2011. A comparison of climate simulations for the last glacial maximum with three different versions of the ECHAM model and implications for summer-green tree refugia. Climate of the Past 7, 91–114. doi:10.5194/cp-7-91-2011

Arsuaga, J. L., Villaverde, V., Quam, R., Gracia, A., Lorenzo, C., Martínez, I., Carretero, J. M., 2002. The Gravettian occipital bone from the site of Malladetes (Barx, Valencia, Spain). Journal of Human Evolution, 43, 381–393.

Auerswald, K., Wittmer, M.H.O.M, Männel, T.T., Bai, Y.F., Schäufele, R., Schnyder, H., 2009. Large regional-scale variation in C3/C4 distribution pattern of Inner Mongolia steppe is revealed by grazer wool carbon isotope composition. Biogeosciences 6, 795–805.

Aura Tortosa, E.J., Jordá Pardo, J.F. and Fortea Perez, F.J., 2006. Cueva de Nerja (Málaga, Espana) y los inicios del solutrense en Andalucia. Zephyrus 59, 67–88.

Ayliffe, L. K., and Chivas, A. R., 1990. Oxygen isotope composition of the bone phosphate of Australian kangaroos: potential as a palaeoenvironmental recorder. Geochimica et Cosmochimica Acta 54, 2603–2609.

Ayliffe, L. K., Lister, A. M., Chivas, A. R., 1992. The preservation of glacial-interglacial climatic signatures in the oxygen isotopes of elephant skeletal phosphate. Palaeogeography, Palaeoclimatology, Palaeoecology 99, 179–191.

Balasse, M., and Ambrose, S. H., 2005. Distinguishing sheep and goats using dental morphology and stable carbon isotopes in C4 grassland environments. Journal of Archaeological Science 32, 691–702.

Balasse, M., Bocherens, H., Mariotti, A., 1999. Intra-bone variability of collagen and apatite isotopic composition used as evidence of a change of diet. Journal of Archaeological Science 26, 593–598.

Barquín, R.M., 2014. La secuencia estratigráfica de la Cueva de El Pendo:(Escobedo de Camargo, Cantabria). in Los cazadores recolectores del Pleistoceno y del Holoceno en Iberia y el estrecho de Gibraltar: estado actual del conocimiento del registro arqueológico. Universidad de Burgos.

Beghin, P., S. Charbit, S., M. Kageyama, M., Combourieu-Nebout, N., Hatté, C., C. Dumas, C., Peterschmitt, J.-Y., 2016. What drives LGM precipitation over the western Mediterranean? A study focused on the Iberian Peninsula and northern Morocco. Climate Dynamics 46, 2611–2631. DOI 10.1007/s00382-015-2720-0

Bekenov, A. B., Grachev, I. A., Milner-Gulland, E. J., 1998. The ecology and management of the saiga antelope in Kazakhstan. Mammal Review 28, 1–52.

Belmaker, M., Hovers, E., 2011. Ecological change and the extinction of the Levantine Neanderthals: implications from a diachronic study of micromammals from Amud Cave, Israel. Quaternary Science Reviews 30, 3196–3209.

Ben-David, M., Shochat, E., Adams, L. G., 2001. Utility of stable isotope analysis in studying foraging ecology of herbivores: examples from moose and caribou. Alces 37, 421–435.

Benetti, M., Reverdin, G., Aloisi, G., Sveinbjörnsdóttir, Á., 2017. Stable isotopes in surface waters of the Atlantic Ocean: Indicators of ocean-atmosphere water fluxes and oceanic mixing processes. Journal of Geophysical Research: Oceans 122, 4723–4742.

Benito Garzón, M., Sánchez de Dios, R., Sáinz Ollero, H., 2007. Predictive modelling of tree species distributions on the Iberian Peninsula during the Last Glacial Maximum and Mid-Holocene. Ecography 30, 120–134.

Berger, J., 1986. Wild horses of the Great Basin: Social Competition and Population Size. Chicago, University of Chicago Press.

Bernard, A., Daux, V., Lécuyer, C., Brugal, J. P., Genty, D., Wainer, K., Gardien, V., Fourel, F., Jaubert, J., 2009. Pleistocene seasonal temperature variations recorded in the $\delta^{18}O$ of *Bison priscus* teeth. Earth and Planetary Science Letters 283, 133–143.

Binney, H., Edwards, M., Macias-Fauria, M., Lozhkin, A., Anderson, P., Kaplan, J. O., Andreev, A., Bezrukova, E., Blyakharchurk, T., Jankovska, V., Khazina, I., Krivonogov, S., Kremenetski, K., Nield, J., Novenko, E., Ryabogina, N., Solovieva, N., Willis, K., Zernitskaya, V., 2017. Vegetation of Eurasia from the last glacial maximum to present: Key biogeographic patterns. Quaternary Science Reviews 157, 80–97.

Blumenthal, S.A., Levin, N.E., Brown, F.H., Brugal, J.-P., Chritz, K.L., Harris, J.M., Jehle, G.E., Cerling, T.E., 2017. Aridity and hominin environments. Proc. Natl. Acad. Sci. 114, 7331–7336.

Blunier, T., and Brook, E. J., 2001. Timing of millennial-scale climate change in Antarctica and Greenland during the last glacial period. Science 291, 109–112.

Bocherens, H., Koch, P. L., Mariotti, A., Geraads, D., Jaeger, J. J., 1996. Isotopic biogeochemistry (^{13}C, ^{18}O) of mammalian enamel from African Pleistocene hominid sites. Palaios 11, 306–318.

Bond, G., Heinrich, H., Broecker, W., Labeyrie, L., McManus, J., Andrews, J., Huon, S., Jantschik, R., Clasen, S., Simet, C., Tedesco, K., Klas, M., Bonani, G., Ivy, S., 1992. Evidence for massive discharges of ice- bergs into the North Atlantic Ocean during the last glacial period. Letters to Nature 360, 245–249.

Bouttes, N., Paillard, D., Roche, D. M., Brovkin, V., Bopp, L., 2011. Last Glacial Maximum CO_2 and $\delta^{13}C$ successfully reconciled. Geophysical Research Letters, 38, L02705, doi:10.1029/2010GL044499

Breuil, H., and Obermaier, H., 1912. Les premiers travaux de l'Institut de Paléontologie Humaine. Masson et Cie.

Bryant, J. D., and Froelich, P. N., 1995. A model of oxygen isotope fractionation in body water of large mammals. Geochimica et Cosmochimica Acta 59, 4523–4537.

961 Bryant, J. D., Koch, P. L., Froelich, P. N., Showers, W. J., Genna, B. J., 1996. Oxygen
962 isotope partitioning between phosphate and carbonate in mammalian apatite. Geochimica
963 et Cosmochimica Acta 60, 5145–5148.
964 Bryant, J. D., Luz, B., Froelich, P. N., 1994. Oxygen isotopic composition of fossil horse
965 tooth phosphate as a record of continental paleoclimate. Palaeogeography,
966 Palaeoclimatology, Palaeoecology 107, 303–316.
967 Bugalho, M. N., and Milne, J. A., 2003. The composition of the diet of red deer (*Cervus*
968 *elaphus*) in a Mediterranean environment: a case of summer nutritional constraint? Forest
969 Ecology and Management 181, 23–29.
970 Burke, A., Kageyama, M., Latombe, G., Fasel, M., Vrac, M., Ramstein, G., James, P. M.,
971 2017. Risky business: The impact of climate and climate variability on human population
972 dynamics in Western Europe during the Last Glacial Maximum. Quaternary Science
973 Reviews 164, 217–229.
974 Burke, A., Levavasseur, G., James, P. M., Guiducci, D., Izquierdo, M. A., Bourgeon, L.,
975 Kageyama, M., Ramstein, G., Vrac, M., 2014. Exploring the impact of climate variability
976 during the Last Glacial Maximum on the pattern of human occupation of Iberia. Journal of
977 Human Evolution 73, 35–46.
978 Cao, J., Wang, B., Liu, J., 2019. Attribution of the Last Glacial Maximum climate
979 formation. Climate Dynamics 53, 1661–1679.
980 Cerling, T. E., and Harris, J. M., 1999. Carbon isotope fractionation between diet and
981 bioapatite in ungulate mammals and implications for ecological and paleoecological
982 studies. Oecologia 120, 347–363.
983 Charette, M. A., and Smith, W. H., 2010. The volume of Earth's ocean. Oceanography 23,
984 112–114.
985 Chenery, C. A., Pashley, V., Lamb, A. L., Sloane, H. J., Evans, J. A., 2012. The oxygen
986 isotope relationship between the phosphate and structural carbonate fractions of human
987 bioapatite. Rapid Communications in Mass Spectrometry 26, 309–319.
988 Christie, A. H. C., 1967. The sensitivity of chamois and red deer to temperature fluctuations.
989 In Proceedings New Zealand Ecological Society 14, 34–39.
990 Clark, P. U., Dyke, A. S., Shakun, J. D., Carlson, A. E., Clark, J., Wohlfarth, B., Mitrovica,
991 J.X., Hostetler, S.W., McCabe, A. M., 2009. The last glacial maximum. Science 325, 710–
992 714.
993 Collins, R.P. and Jones, M.B., 1986. The influence of climatic factors on the distribution of
994 C4 species in Europe. Vegetatio 64, 121–129.
995 Coplen, T. B., Kendall, C., Hopple, J., 1983. Comparison of stable isotope reference
996 samples. Nature 302, 236–238.
997 Cormie, A. B., Luz, B., Schwarcz, H. P., 1994. Relationship between the hydrogen and
998 oxygen isotopes of deer bone and their use in the estimation of relative
999 humidity. Geochimica et Cosmochimica Acta 58, 3439–3449.
1000 Corona, C., Guiot, J., Edouard, J. L., Chalié, F., Büntgen, U., Nola, P., Urbinati, C., 2010.
1001 Millennium-long summer temperature variations in the European Alps as reconstructed
1002 from tree rings. Climate of the Past 6, 379–400.
1003 Crucifix, M., and Hewitt, C. D., 2005. Impact of vegetation changes on the dynamics of the
1004 atmosphere at the Last Glacial Maximum. Climate Dynamics 25, 447–459.
1005 Cuenca-Bescós, G., Melero-Rubio, M., Rofes, J., Martínez, I., Arsuaga, J.L., Blain, H.A.,
1006 López-García, J.M., Carbonell, E., Bermudez de Castro, J.M., 2011. The Early–Middle
1007 Pleistocene environmental and climatic change and the human expansion in Western
1008 Europe: A case study with small vertebrates (Gran Dolina, Atapuerca, Spain). Journal of
1009 Human Evolution 60, 481–491.

D'Angela, D., and Longinelli, A., 1990. Oxygen isotopes in living mammal's bone phosphate: further results. Chemical Geology: Isotope Geoscience section 86, 75–82.
Dansgaard, W., 1964. Stable isotopes in precipitation. Tellus 16, 436–468.
Dansgaard, W., Johnsen, S., Clausen, H., Dahl-Jensen, D., Gundestrup, N., Hammer, C., Hvidberg, C., Steffensen, J., Sveinbjörnsdottir, A., Jouzel, J., Bond, G., 1993. Evidence for general instability of past climate from a 250-kar ice-core record. Nature 364, 218–220.
Daux, V., Lécuyer, C., Adam, F., Martineau, F., Vimeux, F., 2005. Oxygen isotope composition of human teeth and the record of climate changes in France (Lorraine) during the last 1700 years. Climatic Change 70, 445–464.
De la Peña Alonso, P., 2013. Estudio estratigráfico y tecnotipológico de los niveles basales de la cueva de Les Mallaetes (Barx, Valencia): nuevas claves para el Paleolítico superior inicial mediterráneo. Zephyrus 71, 61–88.
De los Terreros, J.Y.S. and Castanedo, A.G., 2010. Las estrategias de subsistencia en la región central de la cornisa cantábrica ¿Continuidad o ruptura? Nivel cero: revista del grupo arqueológico. Attica 12, 35–51.
Delgado-Huertas, A., Iacumin, P., Stenni, B., Chillón, B. S., Longinelli, A., 1995). Oxygen isotope variations of phosphate in mammalian bone and tooth enamel. Geochimica et Cosmochimica Acta 59, 4299–4305.
Delpech, F., 2012. Biostratigraphie des niveaux solutréens de Laugerie-Haute (Les Eyzies, Dordogne, France). Implications archéologiques. PALEO. Revue d'archéologie préhistorique 23, 105–116.
Discamps, E., Jaubert, J., Bachellerie, F., 2011. Human choices and environmental constraints: deciphering the variability of large game procurement from Mousterian to Aurignacian times (MIS 5-3) in southwestern France. Quaternary Science Reviews 30, 2755–2775.
Duplessy, J. C., Labeyrie, L., Waelbroeck, C., 2002. Constraints on the ocean oxygen isotopic enrichment between the Last Glacial Maximum and the Holocene: Paleoceanographic implications. Quaternary Science Reviews 21, 315–330.
Ehleringer, J.R., 2005. On the influence of atmospheric CO_2, temperature, and water on the abundances of C3/C4 taxa. In J.R. Ehleringer, T.E. Cerling, and M.D. Dearing (eds.), A history of atmospheric CO_2 and its effect on plants, animals, and ecosystems. Springer Verlag, New York.
Ehleringer, J.R., 2005. On the influence of atmospheric CO_2, temperature, and water on the abundances of C3/C4 taxa. In J.R. Ehleringer, T.E. Cerling, and M.D. Dearing (eds.), A history of atmospheric CO_2 and its effect on plants, animals, and ecosystems. Springer Verlag, New York
Elenga, H., Peyron, O., Bonnefille, R., Jolly, D., Cheddadi, R., Guiot, J., Andrieu, V., Bottema, S., Buchet, G., de Beaulieu, J.-L., Hamilton, A.C., Maley, J., Marchant, R., Perez-Obiol, R., Reille, M., Riollet, G., Scott, L., Straka, H., Taylor, D., Van Campo, E., Vincens, A., Laarif, F. Johnson, H., 2000. Pollen-based biome reconstruction for southern Europe and Africa 18,000 yr BP. Journal of Biogeography 27, 621–634.
Fabre, M., Lécuyer, C., Brugal, J.-P., Amiot, R., Fourel, F., Martineau, F., 2011. Late Pleistocene climatic change in the French Jura (Gigny) recorded in the $\delta^{18}O$ of phosphate from ungulate tooth enamel. Quaternary Research 75, 605–613.
Farquhar, G. D., O'Leary, M. H., Berry, J. A., 1982. On the relationship between carbon isotope discrimination and the intercellular carbon dioxide concentration in leaves. Functional Plant Biology 9, 121–137.
Ferguson, J. E., Henderson, G. M., Fa, D. A., Finlayson, J. C., Charnley, N. R., 2011. Increased seasonality in the Western Mediterranean during the last glacial from limpet shell geochemistry. Earth and Planetary Science Letters 308, 325–333.

Fortea Perez, J. and Jorda Cerda, F., 1976. La Cueva de Les Mallaetes y los Problemas del Paleolítico Superior del Mediterráneo Español. Zephyrus XXVI-XXVII, 129–166.

Fricke, H. C., Clyde, W. C., O'Neil, J. R., 1998. Intra-tooth variations in δ^{18O} (PO_4) of mammalian tooth enamel as a record of seasonal variations in continental climate variables. Geochimica et Cosmochimica Acta 62, 1839–1850.

Fricke, H.C., O'Neil, J.R., 1999. The correlation between $^{18}O/^{16}O$ ratios of meteoric water and surface temperature: its use in investigating terrestrial climate change over geologic time. Earth and Planetary Science Letters 170, 181–196.

Fu, Q. et al., 2016. The genetic history of ice age Europe. Nature 534, 200–205.

Fumanal, M. and Dupré, M., 1983. Schéma paléoclimatique et chrono-stratigraphique d'une séquence du Paléolithique supérieur de la région de Valence (Espagne). Quaternaire 20, 39–46.

Gat, J.R., Mook, W.G. and Meijer, H.A.J., 2001. Observed isotope effects in precipitations. In Environmental Isotopes in the Hydrological cycle, G. Mook., ed., IHP-V ITechnical Documents in Hydrology I No. 39, Vol. II UNESCO, Paris.

Gerhart, L.M. and Ward, J.K., 2010. Plant responses to low [CO_2] of the past. New Phytologist 188, 674–695.

Goedert, J., Lécuyer, C., Amiot, R., Arnaud-Godet, F., Wang, X., Cui, L., Cuny, G., Douay, G., Fourel, F., Panczer, G., Simon, L., Steyer, J.-S., Zhu, M., 2018. Euryhaline ecology of early tetrapods revealed by stable isotopes. Nature 558, 68–72.

Grafenstein von, U., Erlenkeuser, H., Müller, J., Trimborn, P., Alefs, J., 1996. A 200-year mid-European air temperature record preserved in lake sediments: An extension of the δ^{18}Op-air temperature relation into the past. Geochimica et Cosmochimica Acta 60, 4025–4036.

Grootes, P.M., Stuiver, M., White, J.W.C., Johnsen, S., Jouzel, J., 1993. Comparison of oxygen isotope records from the GISP2 and GRIP Greenland ice cores. Nature 366, 552–554.

Hammer, Ø., Harper, D.A.T., and P. D. Ryan, 2001. PAST: Paleontological Statistics Software Package for Education and Data Analysis. Palaeontologia Electronica 4(1), 9 spp.

Hare, V. J., Loftus, E., Jeffrey, A., Ramsey, C. B., 2018. Atmospheric CO_2 effect on stable carbon isotope composition of terrestrial fossil archives. Nature communications 9, 1–8.

Hatté, C., and Guiot, J., 2005. Palaeoprecipitation reconstruction by inverse modelling using the isotopic signal of loess organic matter: application to the Nußloch loess sequence (Rhine Valley, Germany). Climate Dynamics 25, 315. https://doi.org/10.1007/s00382-005-0034-3

Hatté, C., Gauthier, C., Rousseau, D. D., Antoine, P., Fuchs, M., Lagroix, F., Markovic, S.B., Moine, O., Sima, A., 2013. Excursions to C-4 vegetation recorded in the Upper Pleistocene loess of Surduk (Northern Serbia): an organic isotope geochemistry study. Climate of the Past 9, 1001–1014.

Hayes, A., Kucera, M., Kallel, N., Sbaffi, L., Rohling, E. J., 2005. Glacial Mediterranean sea surface temperatures based on planktonic foraminiferal assemblages. Quaternary Science Reviews 24, 999–1016.

Heinrich, H., 1988. Origin and consequences of cyclic ice rafting in the Northeast Atlantic ocean during the past 130,000 years. Quaternary Research 29, 142–152.

Hernández Fernández, M., Álvarez Sierra, M.Á., Peláez-Campomanes, P., 2007. Bioclimatic analysis of rodent palaeofaunas reveals severe climatic changes in Southwestern Europe during the Plio-Pleistocene. Palaeogeography, Palaeoclimatology, Palaeoecology 251, 500–526.

Hillaire-Marcel, C., Causse, C., 1989. The late Pleistocene Laurentide glacier: ThU dating of its major fluctuations and δ^{18}O range of the ice. Quaternary Research 32, 125–138.

Hoyos Gómez, M., and Laville, H., 1982. Nuevas aportaciones sobre la estratigrafía y sedimentología de los depósitos del Paleolítico Superior de la Cueva de El Pendo (Santander): sus implicaciones. Zephyrus 34–35.

Hughes, P. D., 2018. Little Ice Age glaciers and climate in the Mediterranean mountains: a new analysis. Cuadernos de investigación geográfica/Geographical Research Letters 44, 15–45.

Iacumin, P., Bocherens, H., Mariotti, A., Longinelli, A., 1996. Oxygen isotope analyses of co-existing carbonate and phosphate in biogenic apatite: a way to monitor diagenetic alteration of bone phosphate? Earth and Planetary Science Letters 142, 1–6.

Iacumin, P., Longinelli, A., 2002. Relationship between $\delta^{18}O$ values for skeletal apatite from reindeer and foxes and yearly mean $\delta^{18}O$ values of environmental water. Earth and Planetary Science Letters 201, 213–219.

Ihl, C., and Klein, D. R., 2001. Habitat and diet selection by muskoxen and reindeer in western Alaska. The Journal of Wildlife Management 65, 964–972.

Jansen, E., Overpeck, J., Briffa, K. R., Duplessy, J. C., Joos, F., Masson-Delmotte, V., and others (2007). Paleoclimate. Climate change 2007: the physical science basis; contribution of Working Group I to the Fourth Assessment Report of the Intergovernmental Panel on Climate Change.

Jones, J.R., Marín-Arroyo, A.B., Straus, L.G., Richards, M.P., 2020. Adaptability, resilience and environmental buffering in European Refugia during the Late Pleistocene: Insights from La Riera Cave (Asturias, Cantabria, Spain). Scientific Reports 10, 1217. doi.org/10.1038/s41598-020-57715-2

Jordá Pardo, J.F. and J.E. Aura Tortosa, 2008. 70 fechas para una cueva. revisión crítica de 70 dataciones c14 del Pleistoceno superior y Holoceno de la cueva de Nerja (Málaga, Andalucía, España). Espacio, Tiempo y Forma. Serie I, Nueva época. Prehistoria y Arqueología 1, 239–255.

Jost, A., Lunt, D., Kageyama, M., Abe-Ouchi, A., Peyron, O., Valdes, P. J., Ramstein, G., 2005. High-resolution simulations of the last glacial maximum climate over Europe: a solution to discrepancies with continental palaeoclimatic reconstructions? Climate Dynamics 24, 577–590.

Kageyama, M., Laîné, A., Abe-Ouchi, A., Braconnot, P., Cortijo, E., Crucifix, M., de Vernal, A., Guiot, J., Hewitt, C.D., Kitoh, A., Kucera, M., Marti, O., Ohgaito, R., Otto-Bliesner B., Peltier, W.R., Rosell-Melé, A., Vettoretti, G., Weber, S.L., Yu, Y., MARGO Project members, 2006. Last Glacial Maximum temperatures over the North Atlantic, Europe and western Siberia: a comparison between PMIP models, MARGO sea–surface temperatures and pollen-based reconstructions. Quaternary Science Reviews 25, 2082–2102.

Kageyama, M., Peyron, O., Pinot, S., Tarasov, P., Guiot, J., Joussaume, S., Ramstein, G., 2001. The Last Glacial Maximum climate over Europe and western Siberia: a PMIP comparison between models and data. Climate Dynamics 17, 23–43.

Koch, P. L., Fisher, D. C., Dettman, D., 1989. Oxygen isotope variation in the tusks of extinct proboscideans: a measure of season of death and seasonality. Geology 17, 515–519.

Kohn, M. J. 2010. Carbon isotope compositions of terrestrial C3 plants as indicators of (paleo) ecology and (paleo) climate. Proceedings of the National Academy of Sciences 107, 19691–19695.

Kohn, M. J., 1996. Predicting animal $\delta^{18}O$: accounting for diet and physiological adaptation. Geochimica et Cosmochimica Acta, 60(23), 4811-4829.

Kolodny, Y., Luz, B., Sander, M., Clemens, W. A., 1996. Dinosaur bones: fossils or pseudomorphs? The pitfalls of physiology reconstruction from apatitic fossils. Palaeogeography, Palaeoclimatology, Palaeoecology 126, 161–171.

Kucera, M., Weinelt, M., Kiefer, T., Pflaumann, U., Hayes, A., Weinelt, M., Chen, M.-T., Mix, A.C., Barrows, T.T., Cortijo, E., Duprat, J., Juggins, S., Waelbroeck, C., 2005. Reconstruction of the glacial Atlantic and Pacific sea-surface temperatures from assemblages of planktonic foraminifera: multi-technique approach based on geographically constrained calibration datasets. Quaternary Science Reviews 24, 951-998.

Kuhlemann, J., Rohling, E. J., Krumrei, I., Kubik, P., Ivy-Ochs, S., Kucera, M., 2008. Regional synthesis of Mediterranean atmospheric circulation during the Last Glacial Maximum. Science, 321, 1338–1340.

La Morgia, V., and Bassano, B., 2009. Feeding habits, forage selection, and diet overlap in Alpine chamois (*Rupicapra rupicapra* L.) and domestic sheep. Ecological Research 24, 1043–1050.

Lambeck, K., Rouby, H., Purcell, A., Sun, Y., Sambridge, M., 2014. Sea level and global ice volumes from the Last Glacial Maximum to the Holocene. Proceedings of the National Academy of Sciences 111, 15296–15303.

Langlois, C., Simon, L., Lécuyer, C. H. (2003. Box-modeling of bone and tooth phosphate oxygen isotope compositions as a function of environmental and physiological parameters. Isotopes in Environmental and Health Studies 39, 259–272.

Latombe, G., Burke, A., Vrac, M., Levavasseur, G., Dumas, C., Kageyama, M., Ramstein, G., 2018. Comparison of spatial downscaling methods of general circulation model results to study climate variability during the Last Glacial Maximum. Geoscientific Model Development 11, 2563–2579.

Lécuyer, C., 2013. Water on Earth. John Wiley & Sons, 266 pp.

Lécuyer, C., Bojar, A. V., Daux, V., Legendre, S. (2020). Geographic variations in the slope of the δ^2H–$\delta^{18}O$ meteoric water line over Europe: A record of increasing continentality. Geological Society, London, Special Publications, 507. doi:10.1144/SP507-2020-68.

Lee, J.-E., Fung, I., DePaolo, D.J., Otto-Bliesner, B., 2008. Water isotopes during the Last Glacial Maximum: New general circulation model calculations. Journalof Geophysical Research 113, D19109, doi:10.1029/2008JD009859.

Leng, M. J., 2006. Isotopes in Palaeoenvironmental Research. Dordrecht, Springer.

Leuenberger, M., Siegenthaler, U., Langway, C., 1992. Carbon isotope composition of atmospheric CO2 during the last ice age from an Antarctic ice core. Nature 357, 488–490.

Levin, N. E., Cerling, T. E., Passey, B. H., Harris, J. M., Ehleringer, J. R., 2006. A stable isotope aridity index for terrestrial environments. Proceedings of the National Academy of Sciences 103, 11201-11205.

Lister, A. M., 2004. The impact of Quaternary Ice Ages on mammalian evolution. Philosophical Transactions of the Royal Society of London. Series B: Biological Sciences 359, 221–241.

Ljungqvist, F. C., Zhang, Q., Brattström, G., Krusic, P. J., Seim, A., Li, Q., Zhang, Q. Moberg, A., 2019. Centennial-scale temperature change in last millennium simulations and proxy-based reconstructions. Journal of Climate 32, 2441–2482.

Loncaric, N., Auffret, G.A., Abrantes, F., Baas, J.H., Gaspar, L., Pujol, C., 1998. Late Quaternary sedimentation patterns on the Meriadzek Terrace, Bay of Biscay (ESSCAMP 02 core: 47°N 9°W). Marine Geology 152, 57–73.

Longinelli, A., 1984. Oxygen isotopes in mammal bone phosphate: a new tool for paleohydrological and paleoclimatological research? Geochimica et cosmochimica Acta 48, 385–390.

López-García, J.M., Blain, H.A., Cuenca-Bescós, G., Ruiz-Zapata, M.B., Dorado-Valiño, M., Gil-García, M.J., Valdeolmillos, A., Ortega, A.I., Carretero, J.M., Arsuaga, J.L., de Castro, J.M.B., Carbonell, E., 2010. Palaeoenvironmental and palaeoclimatic

reconstruction of the latest Pleistocene of El Portalón site, Sierra de Atapuerca, northwestern Spain. Palaeogeography, Palaeoclimatology, Palaeoecology 292, 453–464.
Luccarini, S., Mauri, L., Ciuti, S., Lamberti, P., Apollonio, M., 2006. Red deer (*Cervus elaphus*) spatial use in the Italian Alps: home range patterns, seasonal migrations, and effects of snow and winter feeding. Ethology Ecology & Evolution 18, 127–145. doi:10.1080/08927014.2006.9522718
Ludwig, P., Schaffernicht, E.J., Shao, Y., Pinto , J.G., 2016. Regional atmospheric circulation over Europe during the Last Glacial Maximum and its links to precipitation, Journal of Geophysical Research Atmosphere 121, 2130–2145. doi:10.1002/2015JD024444.
Ludwig, P., Shao, Y., Kehl, M., Weniger, G. C., 2018. The Last Glacial Maximum and Heinrich event I on the Iberian Peninsula: A regional climate modelling study for understanding human settlement patterns. Global and Planetary Change 170, 34–47.
Luz, B., and Kolodny, Y., 1985. Oxygen isotope variations in phosphate of biogenic apatites, IV. Mammal teeth and bones. Earth and Planetary Science Letters 75, 29–36.
Luz, B., Cormie, A. B., Schwarcz, H. P., 1990. Oxygen isotope variations in phosphate of deer bones. Geochimica et Cosmochimica Acta 54, 1723–1728.
Macdonald, D. W., 2006. The Encyclopedia of Mammals (3 ed.), Oxford University Press, 936 pp.
Máguas, C., and Brugnoli, E., 1996. Spatial variation in carbon isotope discrimination across the thalli of several lichen species. Plant, Cell & Environment 19, 437–446.
MARGO Project members, Waelbroeck, C., Paul, A., Kucera, M., Rosell-Melé, A., Weinelt, M., Schneider, R., Mix, A., 2009. Constraints on the magnitude and patterns of ocean cooling at the Last Glacial Maximum. Nature Geoscience 2, 127–132.
Masson-Delmotte, V., Kageyama, M., Braconnot, P., Charbit, S., Krinner, G., Ritz, C., Guilyardi, E., Jouzel, J., Abe-Ouchi, A., Crucifix, M., Gladstone, R. M., Hewitt, C.D., Kitoh, A., LeGrande, A.N., Marti, O., Merkel, U., Motoi, T., Ohgaito, R., Otto-Bliesner, B., Pletier, W.R., Ross, I., Valdes, P.J., Vettoretti, G., Weber, S.L., Wolk, F., Yu, Y., 2006. Past and future polar amplification of climate change: climate model intercomparisons and ice-core constraints. Climate Dynamics 26, 513–529.
Mix, A. C., Bard, E., Schneider, R., 2001. Environmental processes of the ice age: land, oceans, glaciers (EPILOG). Quaternary Science Reviews 20, 627–657.
Morales-Molino, C., and García-Antón, M. (2014). Vegetation and fire history since the last glacial maximum in an inland area of the western Mediterranean Basin (Northern Iberian Plateau, NW Spain). Quaternary Research 81, 63–77.
Morgantini, L.E., and Hudson, R. J., 1989. Nutritional Significance of Wapiti (Cervus Elaphus) Migrations to Alpine Ranges in Western Alberta, Canada. Arctic and Alpine Research 21, 288–295.
Nan, Y., Tian, F., Hu, H., Wang, L., Zhao, S., 2019. Stable isotope composition of river waters across the world. Water 11, 1760. Doi:10.3390/w11091760
Navarro-Serrano, F., López-Moreno, J. I., Azorin-Molina, C., Alonso-González, E., Tomás-Burguera, M., Sanmiguel-Vallelado, A., Revuelto, J., Vicente-Serrano, S. M., 2018. Estimation of near-surface air temperature lapse rates over continental Spain and its mountain areas. International Journal of Climatology 38, 3233–3249.
NGRIP members, 2004. High-resolution record of Northern Hemisphere climate extending into the last interglacial period. Nature 431, 147–151.
O'Leary, M. H., 1981. Carbon isotope fractionation in plants. Phytochemistry 20, 553–67.
Park, R., and Epstein, S., 1961. Metabolic fractionation of C^{13} & C^{12} in plants. Plant Physiology 36, 133–138.
Park, R., Epstein, S., 1960. Carbon isotope fractionation during photosynthesis. Geochimica et Cosmochimica Acta 21, 110–26.

Paul, H. A., Bernasconi, S. M., Schmid, D. W., McKenzie, J. A., 2001. Oxygen isotopic composition of the Mediterranean Sea since the Last Glacial Maximum: constraints from pore water analyses. Earth and Planetary Science Letters 192, 1–14.

Peacock, S., Lane, E., Restrepo, J. M., 2006. A possible sequence of events for the generalized glacial-interglacial cycle. Global Biogeochemical Cycles, 20, GB2010, doi:10.1029/2005GB002448.

Pederzani, S. and K. Britton, K. 2019. Oxygen isotopes in bioarchaeology: Principles and applications, challenges and opportunities. Earth-Science Reviews 188, 77–107.

Peyron, O., Guiot, J., Cheddadi, R., Tarasov, P., Reille, M., de Beaulieu, J. L., Bottema, S., Andrieu, V., 1998. Climatic reconstruction in Europe for 18,000 yr BP from pollen data. Quaternary Research 49, 183–196.

Prud'Homme, C., Lécuyer, C., Antoine, P., Hatté, C., Moine, O., Fourel, F., Amiot, R., Martineau, F., Rousseau, D. D. (2018). $\delta^{13}C$ signal of earthworm calcite granules: A new proxy for palaeoprecipitation reconstructions during the Last Glacial in western Europe. Quaternary Science Reviews 179, 158–166.

Pyankov, V.I., Ziegler, H., Akhani, H., Deigele, C. and Lüttge, U., 2010. European plants with C4 photosynthesis: geographical and taxonomic distribution and relations to climate parameters. Botanical Journal of the Linnean Society 163, 283–304.

Quinzin, M. C., Normand, S., Dellicour, S., Svenning, J. C., Mardulyn, P., 2017. Glacial survival of trophically linked boreal species in northern Europe. Proceedings of the Royal Society B: Biological Sciences 284, 20162799. doi.org/10.1098/rspb.2016.2799

Rasmussen, S.O., Bigler, M., Blockley, S.P., Blunier, T., Buchardt, S.L., Clausen, H.B., Cvijanovic, I., Dahl-Jensen, D., Johnsen, S.J., Fischer, H., et al., 2014. A stratigraphic framework for abrupt climatic changes during the Last Glacial period based on three synchronized Greenland ice-core records: refining and extending the INTIMATE event stratigraphy. Quaternary Science Reviews 106, 14–28.

Reimer, P., Austin, W. E. N., Bard, E., Bayliss, A., Blackwell, P. G., Bronk Ramsey, C., Butzin, M., Cheng, H., Lawrence Edwards, R., Friedrich, M., Grootes, P. M., Guilderson, T. P., Hajdas, I., Heaton, T. J., Hogg, A. G., Hughen, K. A., Kromer, B., Manning, S. W., Muscheler, R., Palmer, J. G., Pearson, C., van der Plicht, J., Reimer, R. W., Richards, D.A., Scott, E.M., Southon, J.R., Turney, C.S.M., Wacker, L., Adolphi, F., Büntgen, U., Capano, M., Fahrni, S., Fogtmann-Schulz, A., Friedrich, R., Köhler, P., Kudsk, S., Miyake, F., Olsen, J., Reinig, F., Sakamoto, M., Sookdeo, A., Talamo, S., 2020. The IntCal20 Northern Hemisphere radiocarbon age calibration curve (0-55 cal kBP). Radiocarbon 62, 725–757.

Rey, K., Amiot, R., Lécuyer, C., Koufos, G. D., Martineau, F., Fourel, F., Kostopoulos D.S., Merceron, G., 2013. Late Miocene climatic and environmental variations in northern Greece inferred from stable isotope compositions ($\delta^{18}O$, $\delta^{13}C$) of equid teeth apatite. Palaeogeography, Palaeoclimatology, Palaeoecology 388, 48–57.

Roche, D. M., Dokken, T. M., Goosse, H., Renssen, H., Weber, S. L., 2007. Climate of the Last Glacial Maximum: sensitivity studies and model-data comparison with the LOVECLIM coupled model. Climate of the Past 3, 205–224.

Rodrigo-Gámiz, M., F. Martínez-Ruiz, S.W. Rampen, S. Schouten, Sinninghe Damsté J. S., 2014. Sea surface temperature variations in the western Mediterranean Sea over the last 20 kar: A dual-organic proxy (UK′37and LDI) approach. Paleoceanography 29, 87–98. doi:10.1002/2013PA00246

Rozanski, K., Araguas-Araguas, L., Gonfiantini, R. (1992). Relation between long-term trends of oxygen-18 isotope composition of precipitation and climate. Science 258, 981–985.

Rozanski, K., Sonntag, C., Münnich, K.O., 1982. Factors controlling stable isotope composition of European precipitation. Tellus, 34(2), 142-150. DOI: 10.3402/tellusa.v34i2.10796.

Sanchez Chillón, B., Alberdi, M. T., Leone, G., Bonadonna, F. P., Stenni, B., Longinelli, A., 1994. Oxygen isotopic composition of fossil equid tooth and bone phosphate: an archive of difficult interpretation. Palaeogeography, Palaeoclimatology, Palaeoecology 107, 317–328.

Sánchez-Goñi, M. F., Landais, A., Fletcher, W.J., Naughton, F., Desprat, S., Duprat, J., 2008. Contrasting impacts of Dansgaard-Oeschger events over a western European latitudinal transect modulated by orbital parameters. Quaternary Science Reviews 27, 1136–1151.

Schmidt, S., Andersen, V., Belviso, S., Marty, J. C., 2002. Strong seasonality in particle dynamics of north-western Mediterranean surface waters as revealed by 234Th/238U. Deep Sea Research Part I: Oceanographic Research Papers 49, 1507–1518.

Schmitt, J., Schneider, R., Elsig, J., Leuenberger, D., Lourantou, A., Chappellaz, J., Köhler, P., Joos, F., Stocker, T.F., Leuenberger, M., Fischer, H., 2012. Carbon isotope constraints on the deglacial CO_2 rise from ice cores. Science 336, 711–714.

Schneider von Deimling, T., Ganopolski, A., Held, H., Rahmstorf, S., 2006. How cold was the last glacial maximum? Geophysical Research Letters 33, 14. 10.1029/2006GL026484

Schrag, D. P., Adkins, J. F., McIntyre, K., Alexander, J. L., Hodell, D. A., Charles, C. D., McManus, J. F., 2002. The oxygen isotopic composition of seawater during the Last Glacial Maximum. Quaternary Science Reviews 21, 331–342.

Schubert, B. A., and Jahren, A. H., 2012. The effect of atmospheric CO_2 concentration on carbon isotope fractionation in C3 land plants. Geochimica et Cosmochimica Acta 96, 29–43.

Sima, A., Paul, A., Schulz, M., Oerlemans, J., 2006. Modeling the oxygen-isotopic composition of the North American Ice Sheet and its effect on the isotopic composition of the ocean during the last glacial cycle. Geophysical Research Letters, 33(15). doi.org/10.1029/2006GL026923.

Skrzypek, G., Wiśniewski, A., Grierson, P. F., 2011. How cold was it for Neanderthals moving to Central Europe during warm phases of the last glaciation? Quaternary Science Reviews, 30, 481–487.

Smith, B. N., and Epstein, S., 1971. Two categories of $^{13}C/^{12}C$ ratios for higher plants. Plant Physiology 47, 380–384.

Sommer, R. S., and Nadachowski, A., 2006. Glacial refugia of mammals in Europe: evidence from fossil records. Mammal Review 36, 251–265.

Steele, J. H., Thorpe, S. A., Turekian, K. K., 2009. Elements of physical oceanography: a derivative of the encyclopedia of ocean sciences. Academic Press, 647 pp.

Strandberg, G., Brandefelt, J., Kjellström, M. E., Smith, B., 2011. High-resolution regional simulation of last glacial maximum climate in Europe. Tellus A: Dynamic Meteorology and Oceanography 63, 107–125.

Straus, L. G., 2018. The Pleistocene–Holocene transition in Cantabrian Spain: current reflections on culture change. Journal of Quaternary Science 33, 346–352.

Straus, L. G., 1981. On the habitat and diet of *Cervus elaphus*. Munibe 33, 175–182.

Straus, L. G., 2000. A quarter-century of research on the Solutrean of Vasco-Cantabria, Iberia and beyond. Journal of Anthropological Research 56, 39–58.

Straus, L. G., and Morales, M. R. G., 2012. The Magdalenian settlement of the Cantabrian region (northern Spain): the view from El Mirón Cave. Quaternary International 272, 111–124.

Szostek, K., 2009. Chemical signals and reconstruction of life strategies from ancient human bones and teeth-problems and perspectives. Anthropological Review 72, 3–30.

Tarasov, P. E., Volkova, V. S., Webb III, T., Guiot, J., Andreev, A. A., Bezusko, L. G., Bezusko, T.V., Bykova, G.V., Dorofeyuk, N.I., Kvavadze, E.V., Osipova, I. M., Panova, N.K., Sevastyanov, D.V., 2000. Last glacial maximum biomes reconstructed from pollen and plant macrofossil data from northern Eurasia. Journal of Biogeography 27, 609–620.

Tazioli, A., Cervi, F., Doveri, M., Mussi, M., Deiana, M., Ronchetti, F., 2019. Estimating the Isotopic Altitude Gradient for Hydrogeological Studies in Mountainous Areas: Are the Low-Yield Springs Suitable? Insights from the Northern Apennines of Italy. Water 11, 1764. doi.org/10.3390/w11091764

Tejada-Lara, J. V., MacFadden, B. J., Bermudez, L., Rojas, G., Salas-Gismondi, R., Flynn, J. J., 2018. Body mass predicts isotope enrichment in herbivorous mammals. Proceedings of the Royal Society B: Biological Sciences 285, 20181020. doi.org/10.1098/rspb.2018.1020

Tejero, J.M., Cacho, C., de Quirós, F.B., 2008. Arte mueble en el Auriñaciense cantábrico. Nuevas aportaciones a la contextualización del frontal grabado de la Cueva de Hornos de la Peña (San Felices de Buelna, Cantabria). Trabajos de Prehistoria 65, 115–123.

Texier, J.-P., 2009. Histoire géologique de sites préhistoriques classiques du Périgord : une vision actualisée : la Micoque, la grotte Vaufrey, le Pech de l'Azé I et II, la Ferrassie, l'abri Castanet, le Flageolet, Laugerie Haute. Collection Documents Préhistoriques 25, Paris, Comité des travaux historiques et scientifiques.

Thompson, I. D., Wiebe, P. A., Mallon, E., Rodgers, A. R., Fryxell, J. M., Baker, J. A., Reid, D., 2015. Factors influencing the seasonal diet selection by woodland caribou (*Rangifer tarandus tarandus*) in boreal forests in Ontario. Canadian Journal of Zoology 93, 87–98.

Thunell, R. C., Williams, D. F., 1989. Glacial–Holocene salinity changes in the Mediterranean Sea: hydrographic and depositional effects. Nature 338, 493–496.

Trueman, C., Chenery, C., Eberth, D. A., Spiro, B., 2003. Diagenetic effects on the oxygen isotope composition of bones of dinosaurs and other vertebrates recovered from terrestrial and marine sediments. Journal of the Geological Society 160, 895–901.

Tütken, T., Furrer, H., Vennemann, T. W., 2007. Stable isotope compositions of mammoth teeth from Niederweningen, Switzerland: implications for the Late Pleistocene climate, environment, and diet. Quaternary International 164, 139–150.

Tzedakis, P. C., Hughen, K. A., Cacho, I., Harvati, K. (2007. Placing late Neanderthals in a climatic context. Nature 449, 206–208.

Vallejo, M. D. S., Cantal, J. A. R., Sánchez, M. C., 2005. La fauna de mamíferos del Solutrense en la Cueva de Nerja. Munibe Antropologia-Arkeologia 57, 255–263.

Van Andel, T. H., Davies, W., Weninger, B., 2003. The human presence in Europe during the last glacial period I: human migrations and the changing climate. In: Neanderthals and modern humans in the European landscape during the last glaciation, Editors: T.H. van Andel; W. Davies, pp. 31-56.

Verpoorte, A., Cosgrove, R., Wood, R., Petchey, F., Lenoble, A., Chadelle, J. P., Smith, C., Kamermans, H., Roebroeks, W., 2019. Improving the chronological framework for Laugerie-Haute ouest (dordogne, France). Journal of Archaeological Science: Reports 23, 574–582.

Vigeant, J., Ribot, I., Hélie, J. F., 2017. Dietary habits in New France during the 17th and 18th centuries: An isotopic perspective. American Journal of Physical Anthropology 162, 462–475.

Villaret, J. C., Bon, R., Rivet, A., 1997. Sexual segregation of habitat by the alpine ibex in the French Alps. Journal of Mammalogy 78, 1273–1281.

Wand, S.J.E., Midgley, G.F., Jones, M.H., Curtis, P.S., 1999. Responses of wild C4 and C3 grass (Poaceae) species to elevated atmospheric CO_2 concentration: a meta-analytic test of current theories and perceptions. Global Change Biology 5, 723-741.

Woillez, M., Kageyama, M., Krinner, G., de Noblet-Ducoudré, N., Viovy, N., Mancip, M., 2011. Impact of CO_2 and climate on the Last Glacial Maximum vegetation: results from the ORCHIDEE/IPSL models. Climate of the Past 7, 557–577.

Wren, C. D., and Burke, A., 2019. Habitat suitability and the genetic structure of human populations during the Last Glacial Maximum (LGM) in Western Europe. PloS one 14, 6. doi.org/10.1371/journal.pone.0217996

Yravedra Sainz de los Terreros, J., 2010a. Estrategias de subsistencia en el yavimentio palaeolítico del Ruso (Igollo de Camargo, Cantabria, España). Espacio, Tiempo y Forma. Serie I, Nueva época. Prehistoria y Arqueología 3, 39–58.

Yravedra Sainz de los Terreros, J., 2010b. Zooarqueología y tafonomía del yacimiento de Hornos de la Peña (San Felices de Buelna, Cantabria). Complutum 2, 69–86.

Yravedra, J., and Brugal, J.-Ph., 2005. Essai sur la biodiversité des associations de grands mammifères à la fin du Pléistocène dans le Sud-Ouest de l'Europe. In Homenaje a Jesús Altuna, 139–162. San Sebastian: MUNIBE (Antropologia-Arkeologia).

Yravedra, J., Julien, M. A., Alcaraz-Castano, M., Estaca-Gómez, V., Alcolea-González, J., de Balbín-Behrmann, R., Lécuyer, C., Hillaire-Marcel, C., Burke, A., 2016. Not so deserted… paleoecology and human subsistence in Central Iberia (Guadalajara, Spain) around the Last Glacial Maximum. Quaternary Science Reviews 140, 21–38.

Yurtsever, Y., 1975. Worldwide survey of stable isotopes in precipitation. Report Isotope Hydrology Section. Vienna: International Atomic Energy Agency, 40.

Zazzo, A., Lécuyer, C., Mariotti, A., 2004. Experimentally-controlled carbon and oxygen isotope exchange between bioapatites and water under inorganic and microbially-mediated conditions. Geochimica et Cosmochimica Acta 68, 1–12.

Table captions:

Table 1: Carbon and oxygen isotope compositions of tooth enamel from large herbivorous mammal remains of the LGM recovered from southwest France (Laugerie-Haute), north Spain (El Cierro, El Ruso, El Pendo, Hornos de la Peña), east Spain (Malladetes) and southeast Spain (Nerja). See the Figure 1 for the geographic locations of these archaeological sites. Studied taxa and ^{14}C ages are also provided along with the calculated oxygen isotope compositions of drinking and diet water ($\delta^{18}O_w$) and the carbon isotope composition of their diet ($\delta^{13}C_{diet}$). See the text for more explanations. Calendar ages were determined using the most recent calibration curve data for the Northern Hemisphere, IntCal20 (Reimer et al., 2020). Calibrated date ranges correspond to 92.9% probability (2σ).

Table 2: Synthesis of calculated mean annual air temperatures (MAAT) and mean annual precipitation (MAP) during the LGM, estimated. from the $\delta^{13}C$- and $\delta^{18}O$-values of tooth enamel carbonate from large herbivorous mammal remains.

Figure captions:

Figure 1: Location of the archaeological sites investigated: Laugerie-Haute, in southwestern France; El Cierro in the Province of Asturias, Hornos de la Peña, El Pendo and El Ruso in Cantabria, Nerja in the Province of Málaga and Malladetes, in the Province of Valencia.

Figure 2: Frequency histogram of the calculated $\delta^{13}C$-value of mammal diets. Cervidae and Equidae are represented in blue; Caprinae, in red. The Gaussian curves were obtained by parametric estimation using PAST4.02 software (Hammer et al., 2001). These curves may slightly differ from those obtained by least-squares approximations (performed using 10,000 iterations) according to the general equation of normal distribution as follows: $y = m1 + m2 * exp^{\left(-\frac{(x-m3)^2}{(m4)^2}\right)}$. Constant uncertainties are ±1σ. For Cervidae and Equidae: m1 = 0.35±0.37; m2 = 7.75±1.24; m3 = -24.02±0.06 and m4 = 0.48±0.09 with $R^2 = 0.71$; for Caprinae: m1 = 0.17±0.20; m2 = 8.33±0.62; m3 = -22.46±0.03 and m4 = -0.60±0.05 with $R^2 = 0.92$.

Figure 3: A) Modern and reconstructed MAP (mm yr^{-1}) for the various French and Spanish archaeological sites. Modern cities (Cestas-Pierroton for Laugerie-Haute, Santander for northern Spain, Valencia for Malladates and Almeria for Nerja) in the vicinity of studied sites were ranked according to increasing MAP that roughly follow a S–N geographic trend. See Table 2 for the output of calculation. B) estimated MAP taking into account the lower atmospheric pCO_2 during the LGM relatively to the Holocene (see section 5.2.1 for a detailed explanation).

Figure 4: Present-day linear relationship between the dew point temperature in °C (T_d) and the mean weighted $\delta^{18}O$-value ($\delta^{18}O_{mw}$) of precipitations, extracted from the IAEA/WMO database. The database was filtered to only include meteorological sites above |32°| latitude. T_d is the dew point (°C). The equation of the linear regression is T_d = 1.30(±0.06)$\delta^{18}O_{mw}$ + 15.69(±0.67) with R^2 = 0.83.

Figure 5: Present-day MAAT–$\delta^{18}O_{mw}$ linear relationships extracted from the IAEA/WMO database. A) Global data above 32°N with 15 outliers removed after linear regression analysis: MAAT = 1.42(±0.04)$\delta^{18}O_{mw}$ + 22.02(±0.44); B) Global data for sites above 32°N and with a MAAT > 0°C: MAAT = 1.40(±0.08)$\delta^{18}O_{mw}$ + 21.86(±0.64).

Figure 6: Frequency histogram of $\delta^{18}O$ of meteoric waters calculated from the $\delta^{18}O$ of apatite carbonate from the sampled teeth of Cervidae, Equidae and Caprinae. Archaeological sites located from northern Spain and SW France, are represented in blue while the Mediterranean sites of Malladates and Nerja are represented in red. The Gaussian curves were obtained by parametric estimation using PAST4.02 software (Hammer et al., 2001). These fitting curves may slightly differ from those obtained by least-squares approximations (performed by using 10,000 iterations) according to the general equation of normal distribution as follows: $y = m1 + m2 * exp^{\left(-\frac{(x-m3)^2}{(m4)^2}\right)}$. For Atlantic sites: m1 = 1.35±0.79; m2 = 13.17±1.57; m3 = -9.98±0.09 and m4 = 0.97±0.15 with R^2 = 0.89. For Mediterranean sites: m1 = 0.12±0.84; m2 = 3.74±1.09; m3 = -5.28±0.19 and m4 = 0.97±0.41 with R^2 = 0.70. The constant uncertainties are ±1σ.

1498 Figure 7: Modern and reconstructed MAAT (°C) of the sampled archaeological sites. Modern
1499 cities (Cestas-Pierroton for Laugerie-Haute, Santander for northern Spain, Valencia for
1500 Malladates and Almeria for Nerja) in the vicinity of studied sites were ranked according
1501 to a decreasing MAAT that roughly follow a S–N trend. See Table 2 for the output of
1502 calculation. Temperatures were calculated assuming an oxygen isotope composition of
1503 oceanic surface waters of +0.8‰ (VSMOW).

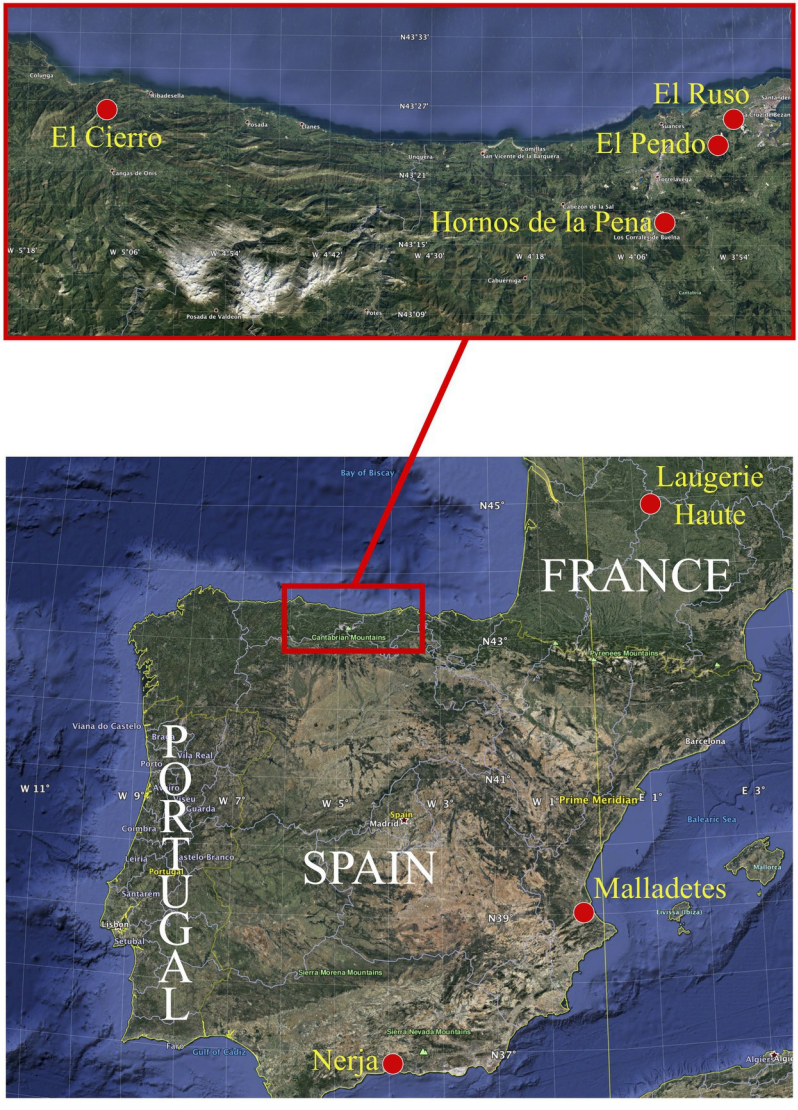
El Cierro
El Ruso
El Pendo
Hornos de la Pena
Laugerie Haute
FRANCE
SPAIN
PORTUGAL
Malladetes
Nerja
Bay of Biscay
Cantabrian Mountains
Pyrenees Mountains
Barcelona
Balearic Sea
Prime Meridian
Sierra Morena Mountains
Sierra Nevada Mountains
Gulf of Cadiz
Lisbon
Madrid
Viana do Castelo
Vila Real
Porto
Aveiro
Guarda
Coimbra
Castelo Branco
Portalegre
Santarém
Setubal
Faro
Mallorca
Ibiza
N45°
N43°
N41°
N39°
N37°
W 11°
W 9°
W 7°
W 5°
W 3°
W 1°
E 1°
E 3°

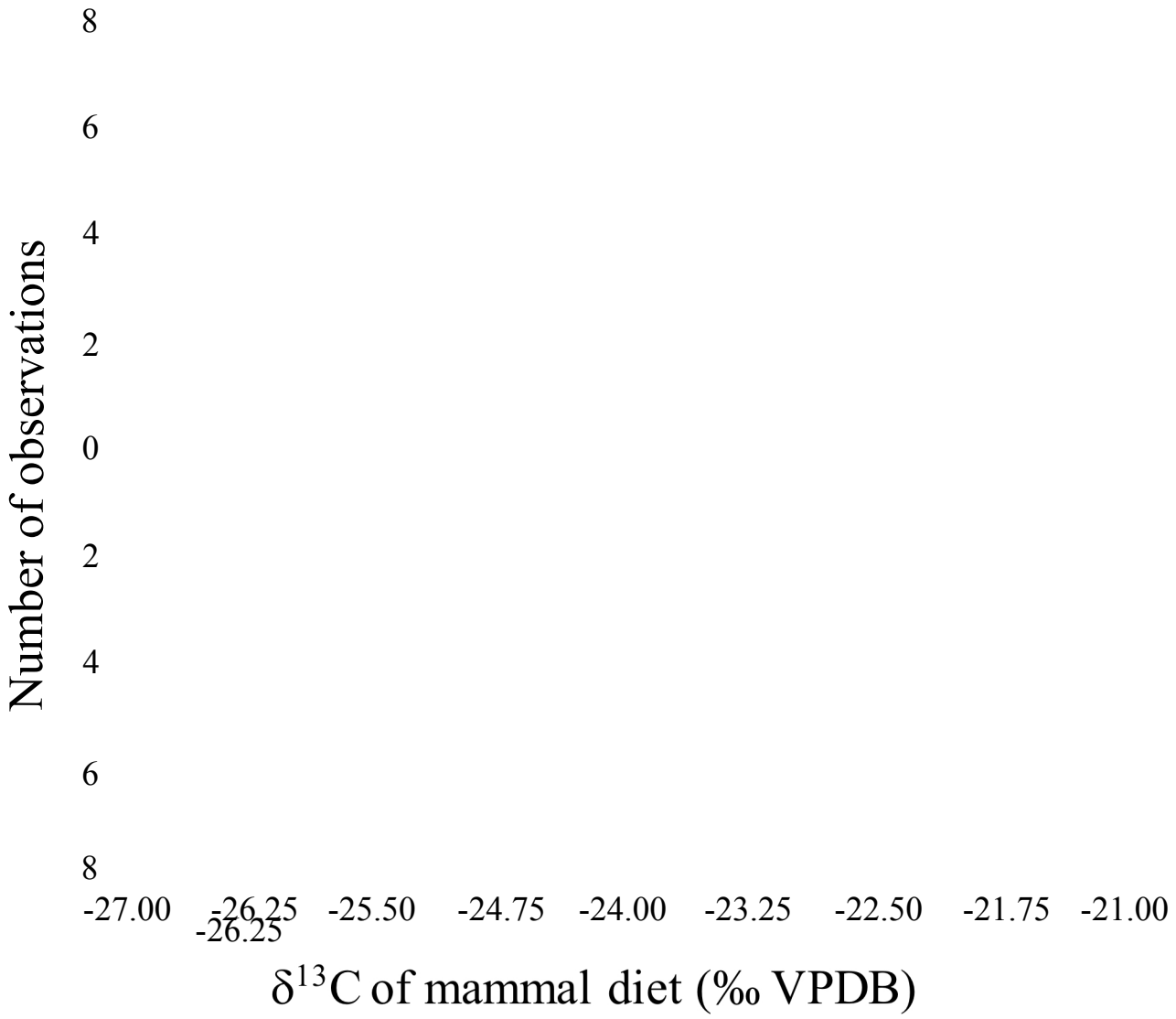
Number of observations
8
6
4
2
0
2
4
6
8
-27.00
-26.25
-25.50
-24.75
-24.00
-23.25
-22.50
-21.75
-21.00
-26.25
δ13C of mammal diet (‰ VPDB)

A)

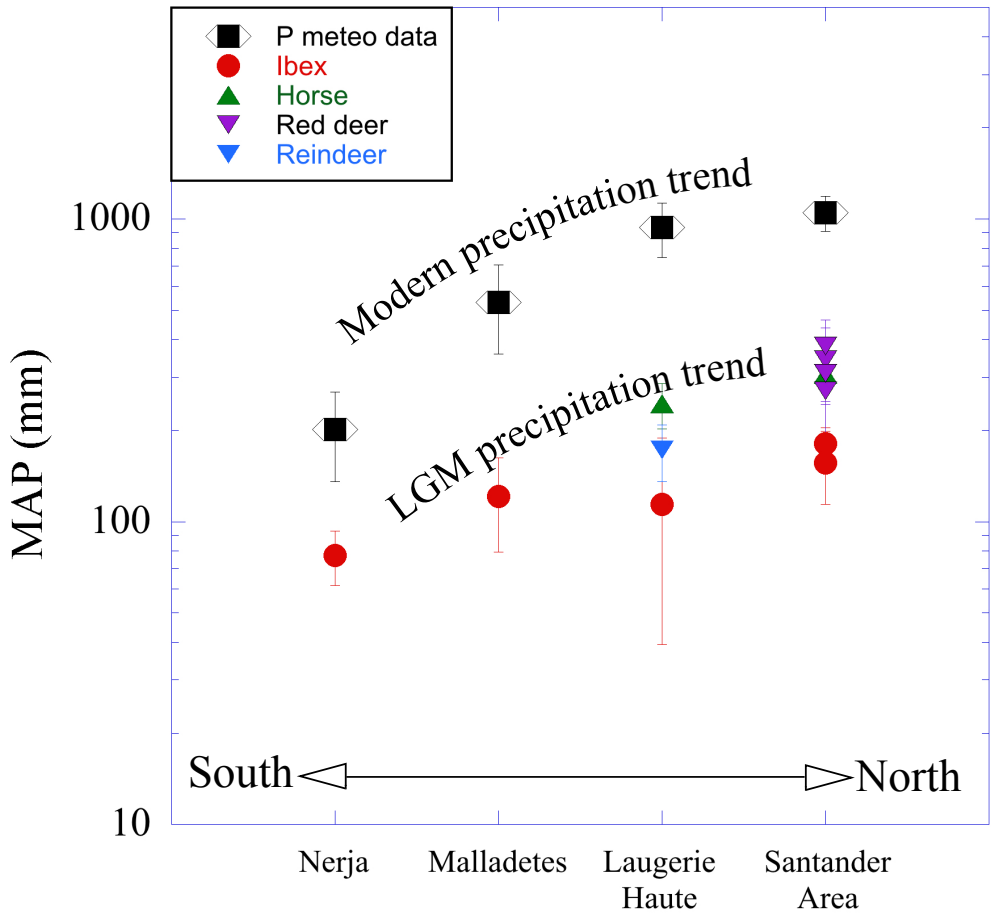
P meteo data
Ibex
Horse
Red deer
Reindeer
Modern precipitation trend
LGM precipitation trend
MAP (mm)
1000
100
10
South
North
Nerja
Malladetes
Laugerie Haute
Santander Area

B)

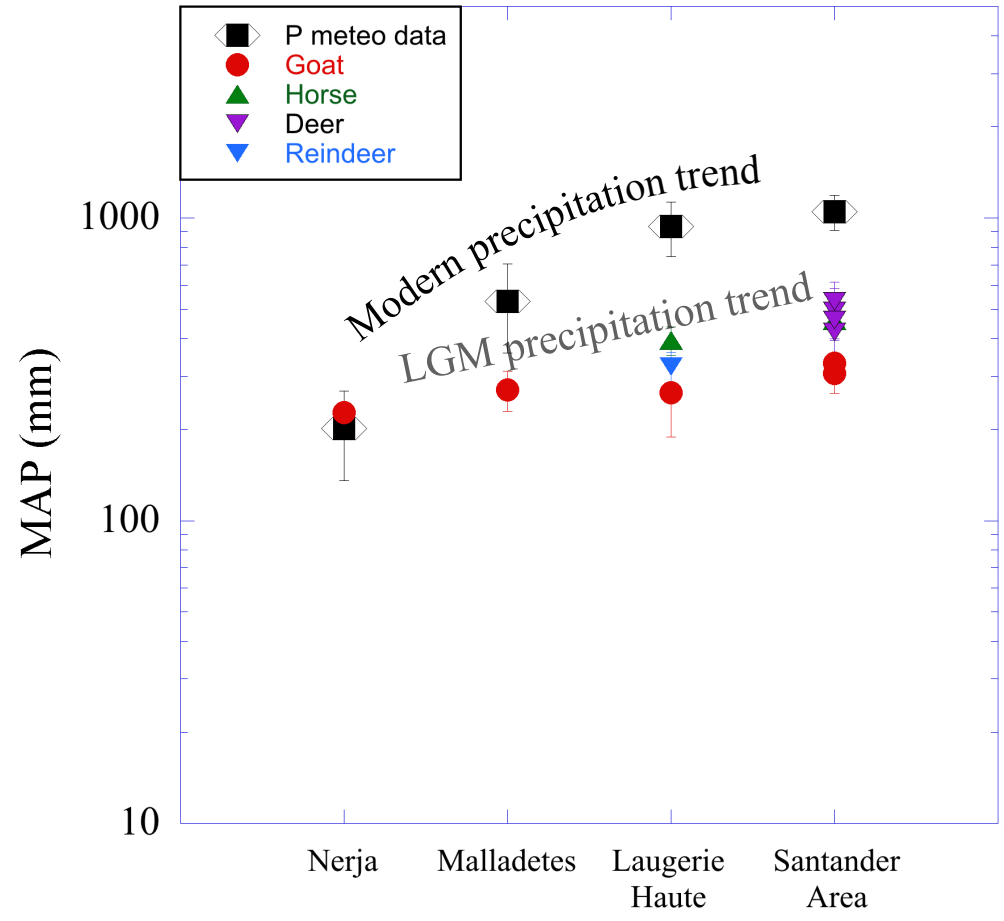
P meteo data
Goat
Horse
Deer
Reindeer
Modern precipitation trend
LGM precipitation trend
MAP (mm)
1000
100
10
Nerja
Malladetes
Laugerie Haute
Santander Area

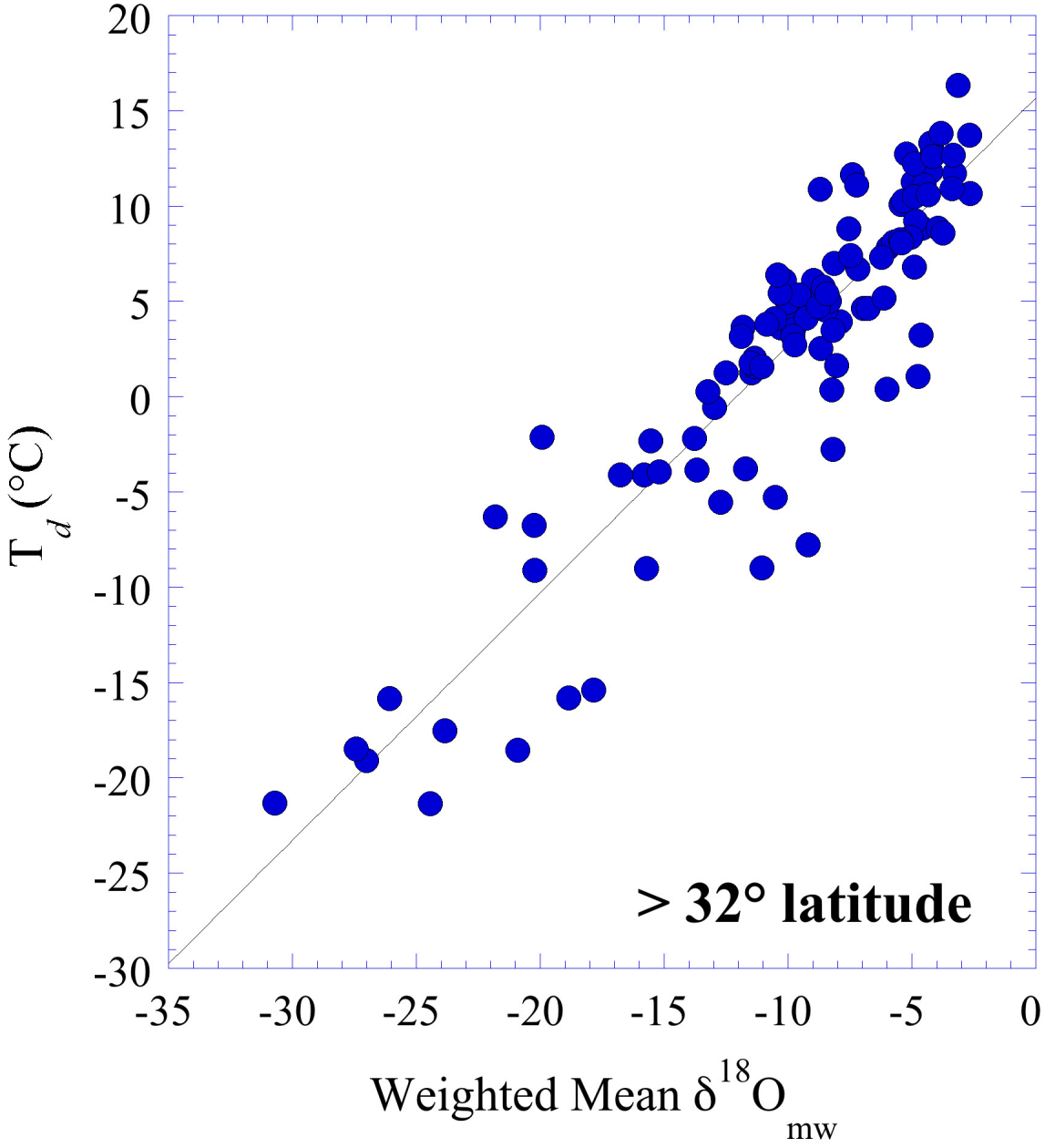
20
15
10
5
0
-5
-10
-15
-20
-25
-30
T_d (°C)
-35
-30
-25
-20
-15
-10
-5
0
Weighted Mean $\delta^{18}O_{mw}$
> 32° latitude

A)

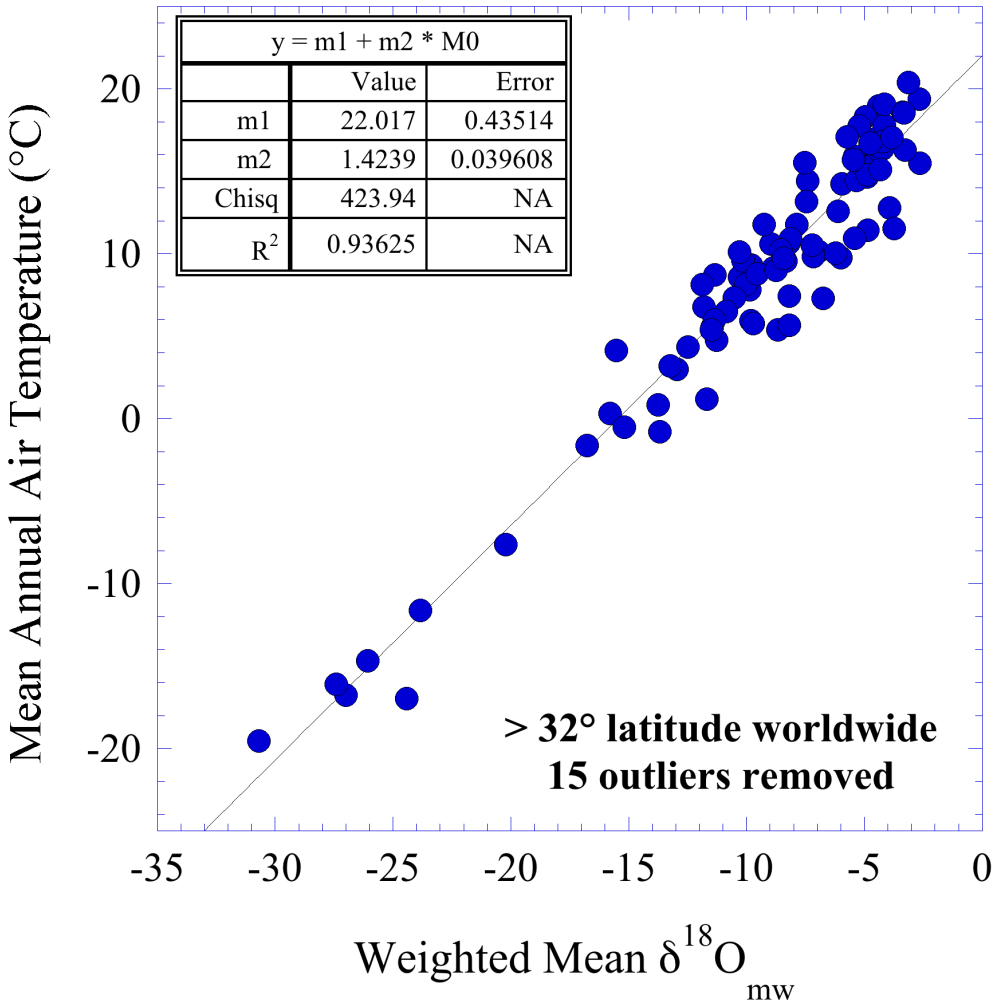
y = m1 + m2 * M0
Value
Error
m1
22.017
0.43514
m2
1.4239
0.039608
Chisq
423.94
NA
R2
0.93625
NA
> 32° latitude worldwide
15 outliers removed
Mean Annual Air Temperature (°C)
Weighted Mean δ18Omw
20
10
0
-10
-20
-35
-30
-25
-20
-15
-10
-5
0

B)

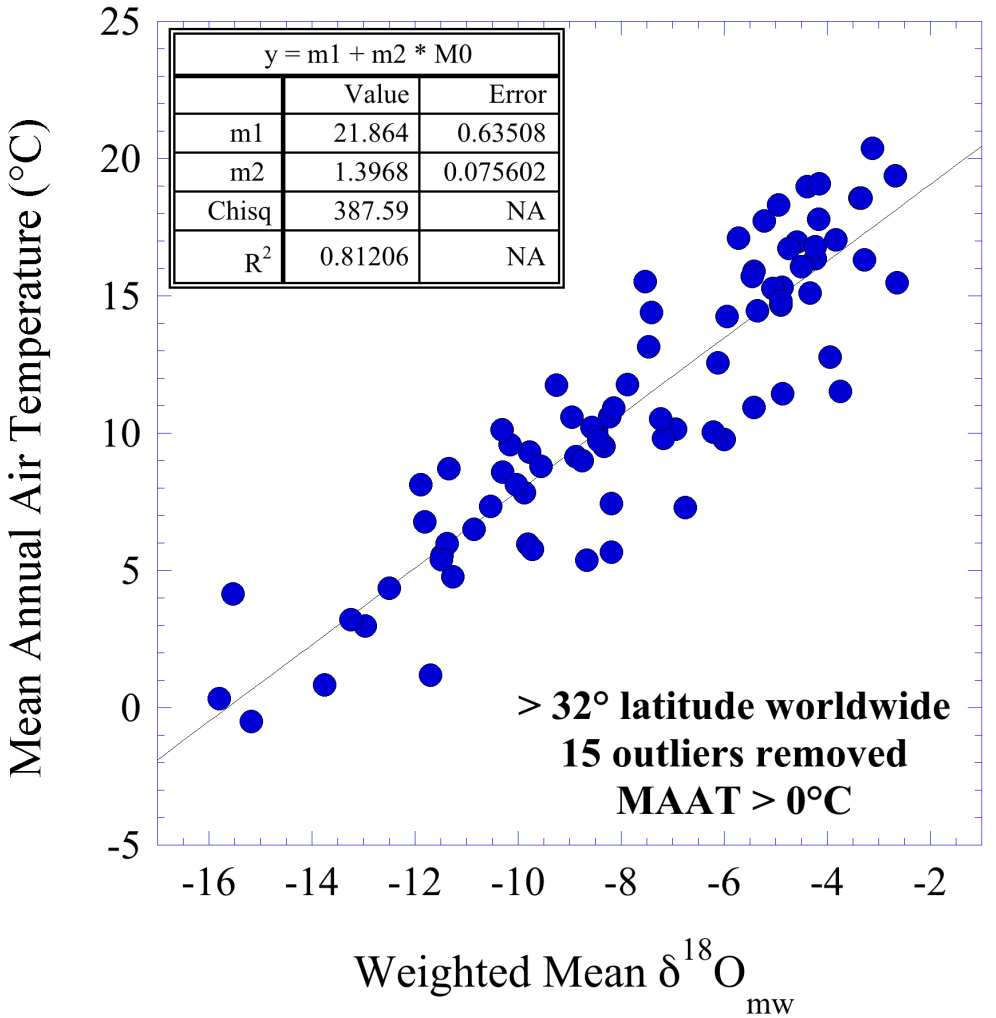
y = m1 + m2 * M0
Value
Error
m1
21.864
0.63508
m2
1.3968
0.075602
Chisq
387.59
NA
R2
0.81206
NA
> 32° latitude worldwide
15 outliers removed
MAAT > 0°C
Mean Annual Air Temperature (°C)
Weighted Mean δ18Omw
25
20
15
10
5
0
-5
-16
-14
-12
-10
-8
-6
-4
-2

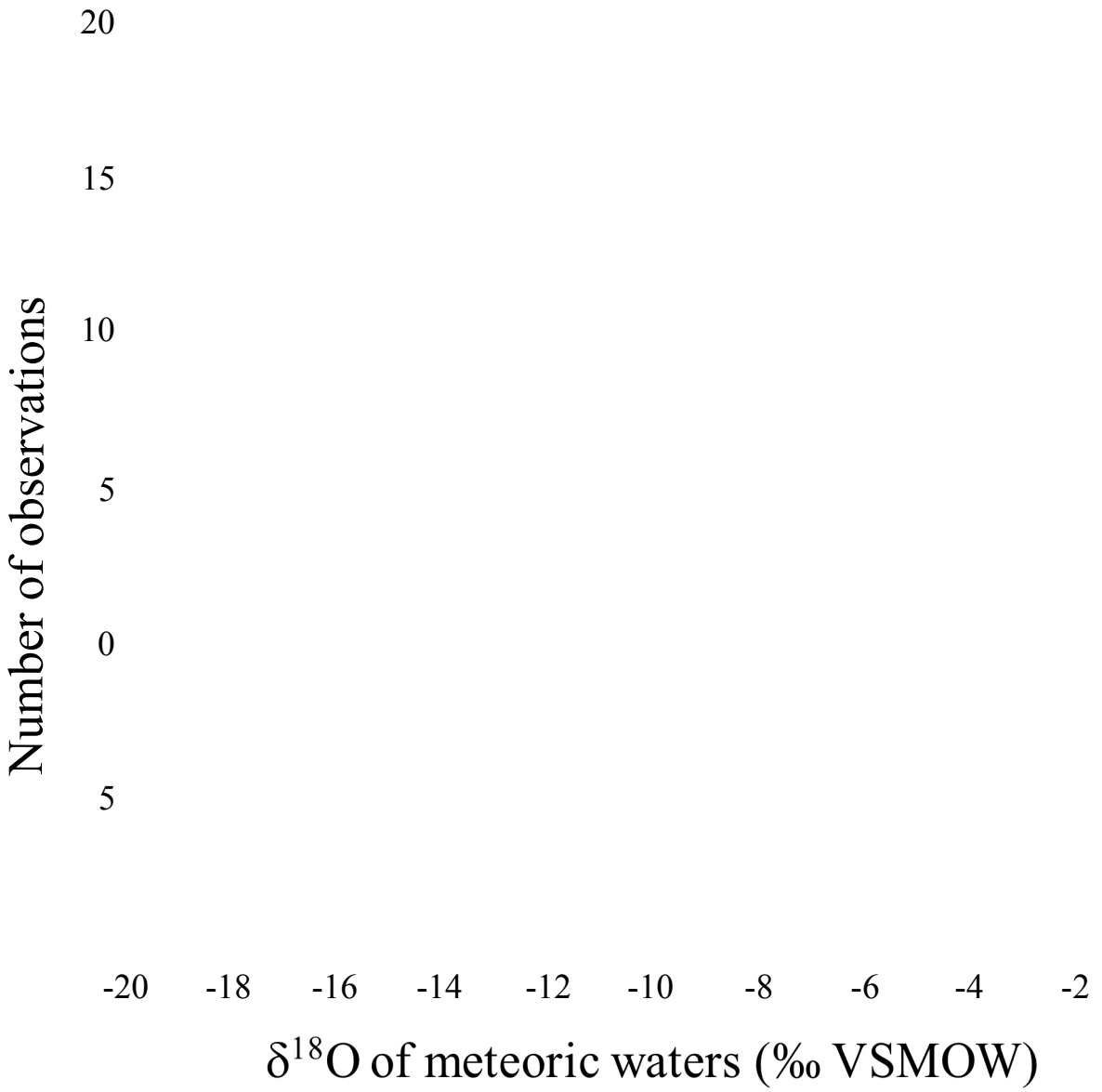
20
15
10
5
0
5
Number of observations
-20
-18
-16
-14
-12
-10
-8
-6
-4
-2
δ18O of meteoric waters (‰ VSMOW)

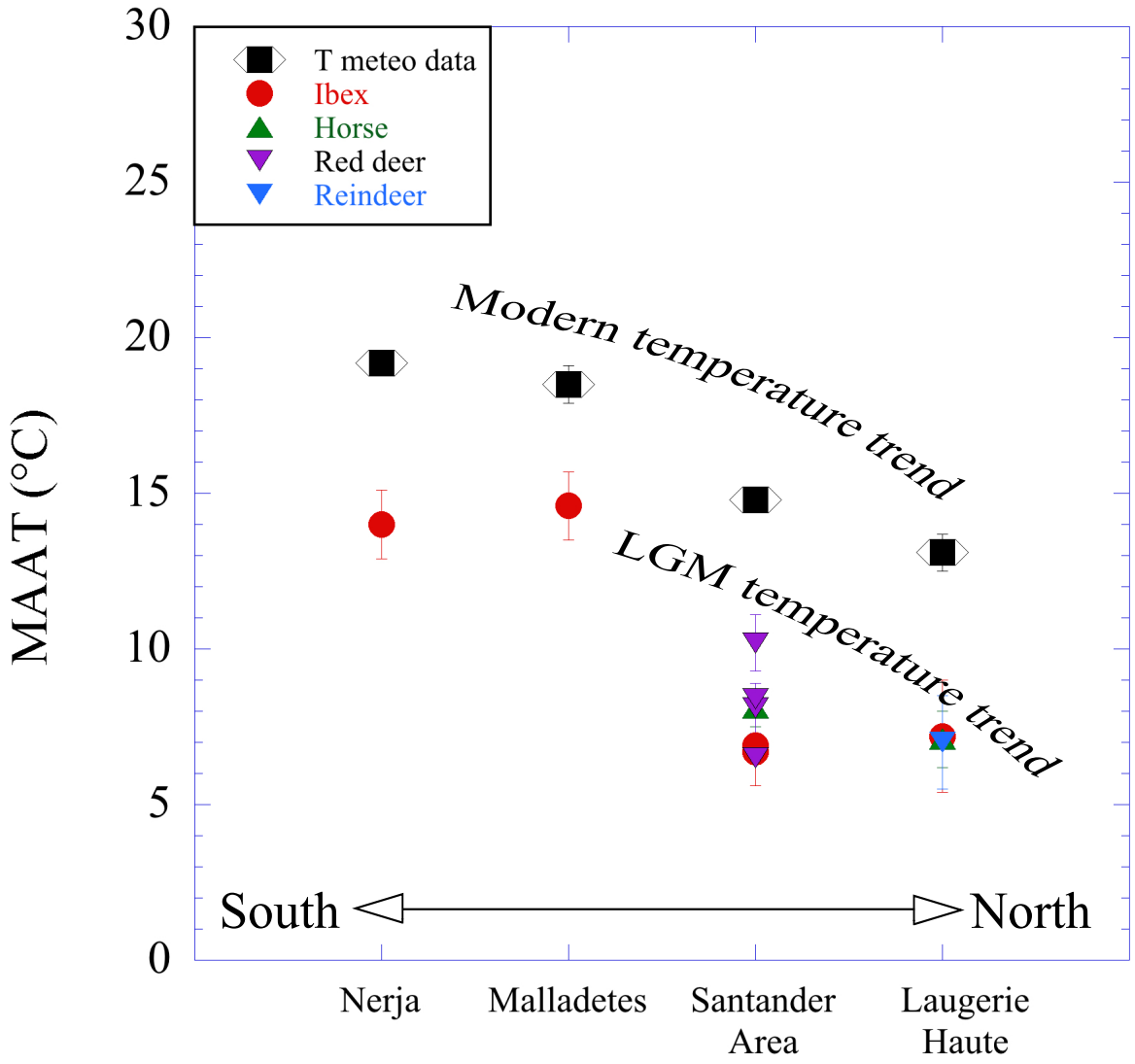
30
25
20
15
10
5
0
MAAT (°C)
T meteo data
Ibex
Horse
Red deer
Reindeer
Modern temperature trend
LGM temperature trend
South
North
Nerja
Malladetes
Santander Area
Laugerie Haute

Site	Lab#	Level	^{14}C dates BP	+/-	^{14}C cal BP IntCal20 (92.9%)	Lithic scale	Taxon	Material	δ^{13}Cc ‰ VPDB	δ^{13}Cdiet ‰ VPDB	Δ^{13}C leaf	P (mm)	δ^{18}Oc ‰ VPDB	δ^{18}Oc ‰ VSMOW	δ^{18}Op calc. ‰ VSMOW	δ^{18}Ow cor.ice (1.2) ‰ VSMOW	δ^{18}Ow cor.ice (0.8) ‰ VSMOW	T (δ^{18}Osw = 1.2) (°C)	T (δ^{18}Osw = 0.8) (°C)
El Cierro	EC-1B	G	15580	75	19011-18735	Lower Magdalenian	*Cervus elaphus*	M3 lower D	-11.21	-24.55	17.99	336	-6.6	24.1	15.1	-10.4	-10.0	6.9	7.5
El Cierro	EC-2B	G	15580	75	19011-18735	Lower Magdalenian	*Cervus elaphus*	M3 lower D	-11.12	-24.46	17.89	323	-6.1	24.5	15.5	-10.0	-9.6	7.4	8.0
El Cierro	EC-3B	G	15580	75	19011-18735	Lower Magdalenian	*Cervus elaphus*	M3 lower D	-10.94	-24.28	17.71	298	-6.6	24.0	15.0	-10.5	-10.1	6.8	7.4
El Cierro	EC-4B	G	15580	75	19011-18735	Lower Magdalenian	*Cervus elaphus*	M3 lower D	-11.42	-24.76	18.22	367	-5.9	24.8	15.8	-9.8	-9.4	7.7	8.3
El Cierro	EC-5B	G	15580	75	19011-18735	Lower Magdalenian	*Cervus elaphus*	M3 lower D	-10.92	-24.26	17.69	296	-6.7	24.0	15.0	-10.5	-10.1	6.8	7.4
El Cierro	EC-17B	G	15580	75	19011-18735	Lower Magdalenian	*Cervus elaphus*	M2 lower D	-12.04	-25.38	18.86	463	-6.2	24.5	15.5	-10.1	-9.7	7.4	8.0
El Cierro	EC-19B	G	15580	75	19011-18735	Lower Magdalenian	*Cervus elaphus*	M2 lower G	-12.28	-25.62	19.11	505	-5.5	25.1	16.1	-9.5	-9.1	8.2	8.8
El Cierro	EC-20B	G	15580	75	19011-18735	Lower Magdalenian	*Cervus elaphus*	M2 lower G	-11.06	-24.40	17.84	315	-4.8	25.9	16.9	-8.8	-8.4	9.2	9.8
El Cierro	EC-21B	G	15580	75	19011-18735	Lower Magdalenian	*Capra pyreneica*	M3 lower G	-10.46	-23.30	16.69	182	-6.3	24.3	15.3	-11.0	-10.6	6.1	6.7
El Cierro	EC-22B	G	15580	75	19011-18735	Lower Magdalenian	*Capra pyreneica*	M2 lower G	-10.67	-23.51	16.91	205	-6.0	24.7	15.7	-10.5	-10.1	6.7	7.3
El Cierro	EC-6B	G1	16360	55	19891-19566	Lower Magdalenian	*Cervus elaphus*	M2 lower G	-11.19	-24.53	17.97	333	-6.2	24.4	15.5	-10.1	-9.7	7.3	7.9
El Cierro	EC-7B	G1	16360	55	19891-19566	Lower Magdalenian	*Cervus elaphus*	M2 lower D	-11.43	-24.77	18.22	367	-6.3	24.3	15.3	-10.2	-9.8	7.2	7.8
El Cierro	EC-9B	G1	16360	55	19891-19566	Lower Magdalenian	*Cervus elaphus*	M3 lower D	-10.43	-23.77	17.18	236	-6.0	24.7	15.7	-9.9	-9.5	7.7	8.3
El Cierro	EC-10B	G1	16360	55	19891-19566	Lower Magdalenian	*Cervus elaphus*	M2 lower G	-11.48	-24.82	18.28	375	-6.6	24.1	15.1	-10.4	-10.0	6.9	7.5
El Cierro	EC-11B	G1	16360	55	19891-19566	Lower Magdalenian	*Cervus elaphus*	M3 lower G	-11.58	-24.92	18.38	390	-6.4	24.3	15.3	-10.2	-9.8	7.2	7.8
El Cierro	EC-12B	G1	16360	55	19891-19566	Lower Magdalenian	*Cervus elaphus*	M2 lower G	-10.73	-24.07	17.50	272	-5.8	24.9	15.9	-9.7	-9.3	7.9	8.5
El Cierro	EC-13B	G1	16360	55	19891-19566	Lower Magdalenian	*Cervus elaphus*	M3 lower G	-11.10	-24.44	17.88	321	-6.0	24.7	15.7	-9.9	-9.5	7.7	8.3
El Cierro	EC-14B	G1	16360	55	19891-19566	Lower Magdalenian	*Cervus elaphus*	M2 lower G	-10.98	-24.32	17.75	304	-6.2	24.5	15.5	-10.1	-9.7	7.4	8.0
El Cierro	EC-15B	G1	16360	55	19891-19566	Lower Magdalenian	*Cervus elaphus*	M3 lower G	-10.99	-24.33	17.77	306	-6.5	24.2	15.2	-10.4	-10.0	7.0	7.6
El Cierro	EC-23B	G1	16360	55	19891-19566	Lower Magdalenian	*Capra pyreneica*	M2 lower G	-10.33	-23.17	16.56	169	-6.6	24.1	15.1	-11.2	-10.8	5.8	6.4
El Cierro	EC-24E	H	LGM	N/A	N/A	Upper Solutrean	*Capra pyreneica*	M2 lower G	-8.93	-21.77	15.09	44	-6.4	24.3	15.3	-11.0	-10.6	6.0	6.6
El Pendo	PE-1B	4	LGM	N/A	N/A	Upper Solutrean	*Cervus elaphus*	M2/M3? upper G	-10.66	-24.00	17.42	263	-6.1	24.6	15.6	-10.0	-9.6	7.5	8.1
El Pendo	PE-2B	4	LGM	N/A	N/A	Upper Solutrean	*Cervus elaphus*	M2 upper G	-10.80	-24.14	17.56	280	-5.5	25.2	16.2	-9.4	-9.0	8.3	8.9
El Pendo	PE-3B	4	LGM	N/A	N/A	Upper Solutrean	*Cervus elaphus*	M3 upper D	-10.52	-23.86	17.27	246	-5.4	25.3	16.3	-9.4	-9.0	8.4	9.0
El Pendo	PE-4B	4	LGM	N/A	N/A	Upper Solutrean	*Cervus elaphus*	M2 upper G	-10.57	-23.91	17.33	252	-6.2	24.5	15.5	-10.1	-9.7	7.4	8.0
El Pendo	PE-5B	4	LGM	N/A	N/A	Upper Solutrean	*Cervus elaphus*	M3 upper G	-10.51	-23.85	17.26	244	-5.4	25.3	16.3	-9.3	-8.9	8.4	9.0
El Pendo	PE-6B	4	LGM	N/A	N/A	Upper Solutrean	*Cervus elaphus*	M3 upper D	-11.04	-24.38	17.81	312	-6.1	24.6	15.6	-10.0	-9.6	7.5	8.1
El Pendo	PE-7B	4	LGM	N/A	N/A	Upper Solutrean	*Cervus elaphus*	M2 upper D	-10.90	-24.24	17.67	294	-6.1	24.6	15.6	-10.0	-9.6	7.5	8.1
El Ruso	RU-2B	3	16410	210	< 20396 - 19322	Upper Solutrean	*Cervus elaphus*	M3 upper G	-10.50	-23.84	17.25	243	-3.7	27.1	18.0	-7.9	-7.5	10.5	11.1
El Ruso	RU-3B	3	16410	210	< 20396 - 19322	Upper Solutrean	*Cervus elaphus*	M2 upper D	-10.59	-23.93	17.35	255	-4.3	26.5	17.4	-8.4	-8.0	9.8	10.4
El Ruso	RU-5B	3	16410	210	< 20396 - 19322	Upper Solutrean	*Cervus elaphus*	M2 upper G	-12.89	-26.23	19.75	622	-3.7	27.1	18.0	-7.8	-7.4	10.5	11.1
El Ruso	RU-6B	3	16410	210	< 20396 - 19322	Upper Solutrean	*Cervus elaphus*	M3 upper G	-10.58	-23.92	17.33	253	-4.6	26.1	17.1	-8.7	-8.3	9.4	10.0
El Ruso	RU-7B	3	16410	210	< 20396 - 19322	Upper Solutrean	*Cervus elaphus*	M2 upper G	-10.84	-24.18	17.60	285	-4.9	25.8	16.8	-8.9	-8.5	9.0	9.6
El Ruso	RU-8B	3	16410	210	< 20396 - 19322	Upper Solutrean	*Cervus elaphus*	M1 upper G	-10.11	-23.45	16.84	198	-5.6	25.1	16.1	-9.6	-9.2	8.1	8.7
Hornos de la Peña	HP-1e	B	18450	520	23425-21038	Lower Magdalenian	*Cervus elaphus*	M3 lower G	-11.52	-24.86	18.31	380	-7.4	23.2	14.3	-11.2	-10.8	5.9	6.5
Hornos de la Peña	HP-4B	B	18450	520	23425-21038	Lower Magdalenian	*Capra pyreneica*	M2 lower D	-9.64	-22.48	15.84	103	-6.7	23.9	14.9	-11.4	-11.0	5.5	6.1
Hornos de la Peña	HP-5B	B	18450	520	23425-21038	Lower Magdalenian	*Capra pyreneica*	M3 lower D	-9.98	-22.82	16.19	134	-6.8	23.9	14.9	-11.4	-11.0	5.5	6.1
Hornos de la Peña	HP-6B	B	18450	520	23425-21038	Lower Magdalenian	*Capra pyreneica*	M2 lower D	-10.00	-22.84	16.21	136	-5.3	25.4	16.4	-9.8	-9.4	7.7	8.3
Hornos de la Peña	HP-7e	B	18450	520	23425-21038	Lower Magdalenian	*Capra pyreneica*	M3 upper D	-10.71	-23.55	16.95	210	-6.1	24.5	15.6	-10.7	-10.3	6.5	7.1
Hornos de la Peña	HP-7b	B	18450	520	23425-21038	Lower Magdalenian	*Capra pyreneica*	M3 upper D	-10.92	-23.76	17.16	233	-6.1	24.6	15.6	-10.7	-10.3	6.5	7.1
Hornos de la Peña	HP-8B	B	18450	520	23425-21038	Lower Magdalenian	*Equus caballus*	M3 lower D	-10.78	-24.28	17.71	299	-5.9	24.8	15.8	-9.8	-9.4	7.8	8.4
Hornos de la Peña	HP-9B	B	18450	520	23425-21038	Lower Magdalenian	*Equus caballus*	M3 lower G	-10.90	-24.40	17.84	315	-6.3	24.4	15.4	-10.3	-9.9	7.1	7.7
Hornos de la Peña	HP-11B	B	18450	520	23425-21038	Lower Magdalenian	*Rupicapra rupicapra*	M3 upper D	-9.90	-22.74	16.11	126	-7.2	23.5	14.5	-11.9	-11.5	4.9	5.5
Hornos de la Peña	HP-12B	B	18450	520	23425-21038	Lower Magdalenian	*Rupicapra rupicapra*	M3 upper D	-10.40	-23.24	16.63	176	-5.3	25.4	16.4	-9.9	-9.5	7.7	8.3
Hornos de la Peña	HP-13B	B	18450	520	23425-21038	Lower Magdalenian	*Rupicapra rupicapra*	M3 lower D	-9.97	-22.81	16.17	133	-7.4	23.2	14.3	-12.1	-11.7	4.5	5.1
Hornos de la Peña	HP-14B	B	18450	520	23425-21038	Lower Magdalenian	*Rupicapra rupicapra*	M2 lower D	-10.22	-23.06	16.44	158	-5.2	25.5	16.5	-9.7	-9.3	7.9	8.5
Laugerie-Haute E.	LH-2B	4 to 8	>17000<19000	N/A	N/A	Magdalenian II	*Capra pyreneica*	M2 upper G	-9.24	-22.08	15.42	69	-4.4	26.3	17.3	-8.9	-8.5	9.1	9.7
Laugerie-Haute E.	LH-3B	4 to 8	>17000<19000	N/A	N/A	Magdalenian II	*Capra pyreneica*	M2 lower D	-10.82	-23.66	17.06	222	-6.2	24.4	15.4	-10.9	-10.5	6.3	6.9
Laugerie-Haute E.	LH-4B	4 to 8	>17000<19000	N/A	N/A	Magdalenian II	*Saiga tatarica*	M3 lower G	-10.45	-22.85	16.22	137	-5.5	25.2	16.2	-10.1	-9.7	7.4	8.0
Laugerie-Haute E.	LH-5B	4 to 8	>17000<19000	N/A	N/A	Magdalenian II	*Saiga tatarica*	M3 lower D	-10.17	-22.57	15.93	111	-4.5	26.2	17.2	-8.9	-8.5	9.0	9.6
Laugerie-Haute E.	LH-6B	4 to 8	>17000<19000	N/A	N/A	Magdalenian II	*Saiga tatarica*	M2 lower D	-9.87	-22.27	15.62	85	-7.4	23.3	14.3	-12.1	-11.7	4.5	5.1
Laugerie-Haute E.	LH-7B	4 to 8	>17000<19000	N/A	N/A	Magdalenian II	*Saiga tatarica*	M3 lower G	-9.70	-22.10	15.44	70	-6.2	24.4	15.4	-10.9	-10.5	6.3	6.9
Laugerie-Haute E.	LH-8B	4 to 8	>17000<19000	N/A	N/A	Magdalenian II	*Saiga tatarica*	M3 lower G	-10.56	-22.96	16.34	148	-5.3	25.4	16.4	-9.8	-9.4	7.7	8.3
Laugerie-Haute E.	LH-14B	4 to 8	>17000<19000	N/A	N/A	Magdalenian II	*Saiga tatarica*	M3 lower G	-10.19	-22.59	15.95	112	-5.5	25.2	16.2	-10.0	-9.6	7.5	8.1
Laugerie-Haute E.	LH-15B	4 to 8	>17000<19000	N/A	N/A	Magdalenian II	*Saiga tatarica*	M2 lower G	-10.14	-22.54	15.89	108	-7.4	23.2	14.2	-12.2	-11.8	4.4	5.0
Laugerie-Haute E.	LH-9B	18 to 20	18260	360	22971-21203	Magdalenian 0	*Saiga tatarica*	M3 upper G	-10.55	-22.95	16.33	147	-5.0	25.7	16.7	-9.5	-9.1	8.3	8.9
Laugerie-Haute E.	LH-13B	18 to 20	18260	360	22971-21203	Magdalenian 0	*Rupicapra rupicapra*	M3 lower G	-9.52	-22.36	15.71	92	-5.6	25.1	16.1	-10.2	-9.8	7.2	7.8
Laugerie-Haute E.	LH-10B	18 to 20	18260	360	22971-21203	Magdalenian 0	*Equus caballus*	M3 upper D	-10.59	-24.09	17.51	274	-6.3	24.3	15.3	-10.3	-9.9	7.0	7.6
Laugerie-Haute E.	LH-11B	18 to 20	18260	360	22971-21203	Magdalenian 0	*Equus caballus*	M3 upper D	-10.10	-23.60	17.00	215	-7.0	23.6	14.7	-11.0	-10.6	6.0	6.6
Laugerie-Haute E.	LH-12B	10 to 16	LGM	N/A	N/A	Magdalenian I	*Capra pyreneica*	M3 lower G	-9.66	-22.50	15.86	105	-7.0	23.6	14.7	-11.7	-11.3	5.1	5.7
Laugerie-Haute E.	LH-16B	10 to 16	LGM	N/A	N/A	Magdalenian I	*Rangifer tarandus*	M3 lower G	-9.92	-23.26	16.64	178	-7.7	22.9	14.0	-10.7	-10.3	6.5	7.1
Laugerie-Haute E.	LH-17B	10 to 16	LGM	N/A	N/A	Magdalenian I	*Rangifer tarandus*	M3 lower G	-10.18	-23.52	16.92	206	-6.9	23.7	14.7	-9.8	-9.4	7.8	8.4
Laugerie-Haute E.	LH-18B	10 to 16	LGM	N/A	N/A	Magdalenian I	*Rangifer tarandus*	M3 lower G	-9.47	-22.81	16.18	133	-8.7	21.9	13.0	-11.9	-11.5	4.9	5.5
Malladetes	MA-1B	7 entry D	25120	240	> 25822-24366 < 29969-28917	Gravettian	*Capra pyreneica*	M3 lower D	-9.18	-22.02	15.36	64	-1.4	29.4	20.3	-5.5	-5.1	13.8	14.4
Malladetes	MA-2B	7 entry D	25120	240	> 25822-24366 < 29969-28917	Gravettian	*Capra pyreneica*	M3 sup G	-9.74	-22.58	15.94	111	-1.8	29.0	19.9	-6.0	-5.6	13.2	13.8
Malladetes	MA-3B	7 E	25120	240	> 25822-24366 < 29969-28917	Gravettian	*Capra pyreneica*	M3 lower G	-10.84	-23.68	17.08	225	-2.2	28.6	19.5	-6.4	-6.0	12.5	13.1
Malladetes	MA-4B	7 E	25120	240	> 25822-24366 < 29969-28917	Gravettian	*Capra pyreneica*	M3 sup D	-9.70	-22.54	15.90	108	-1.3	29.5	20.4	-5.4	-5.0	13.9	14.5
Malladetes	MA-5B	8 E	25120	240	> 25822-24366 < 29969-28917	Gravettian	*Capra pyreneica*	M3 lower D	-9.93	-22.77	16.13	129	-0.7	30.1	21.0	-4.8	-4.4	14.9	15.5
Malladetes	MA-6B	8 E	25120	240	> 25822-24366 < 29969-28917	Gravettian	*Capra pyreneica*	M3 lower G	-9.73	-22.57	15.93	111	-0.7	30.1	21.0	-4.8	-4.4	14.9	15.5
Malladetes	MA-7B	9 entry D	25120	240	> 25822-24366 < 29969-28917	Gravettian	*Capra pyreneica*	M3 sup G	-9.84	-22.68	16.05	121	-2.0	28.8	19.7	-6.2	-5.8	12.9	13.5
Malladetes	MA-8B	9 entry D	25120	240	> 25822-24366 < 29969-28917	Gravettian	*Capra pyreneica*	M3 lower G	-9.62	-22.46	15.81	101	-0.1	30.7	21.6	-4.1	-3.7	15.8	16.4
Nerja	NE-1B	Vest VIIIc A-7	17940	200	> 22311-21181 < 23420-20987	Solutrean	*Capra pyreneica*	M3 lower G	-9.49	-22.33	15.68	90	-1.3	29.5	20.4	-5.5	-5.1	13.9	14.5
Nerja	NE-2B	Vest VIIIc A-7	17940	N/A	> 22311-21181 < 23420-20987	Solutrean	*Capra pyreneica*	M3 lower G	-9.25	-22.09	15.43	69	-0.7	30.2	21.1	-4.7	-4.3	14.9	15.5
Nerja	NE-4B	Vest VIIIc A-7	17940	N/A	> 22311-21181 < 23420-20987	Solutrean	*Capra pyreneica*	M3 lower D	-9.07	-21.91	15.25	55	-1.8	29.0	19.9	-6.0	-5.6	13.2	13.8
Nerja	NE-6B	Vest VIIIc A-7	17940	N/A	> 22311-21181 < 23420-20987	Solutrean	*Capra pyreneica*	M2 lower D	-9.21	-22.05	15.39	66	-1.6	29.2	20.1	-5.8	-5.4	13.4	14.0
Nerja	NE-3B	N84 VIIIe A7-8 & B7-8	17940	N/A	> 22311-21181 < 23420-20987	Solutrean	*Capra pyreneica*	M3 lower G	-9.52	-22.36	15.71	92	-2.8	28.0	18.9	-7.0	-6.6	11.7	12.3
Nerja	NE-5B	N84 VIIIe A7-8 & B7-8	17940	N/A	> 22311-21181 < 23420-20987	Solutrean	*Capra pyreneica*	M3 lower D	-9.52	-22.36	15.71	92	-1.7	29.1	20.0	-5.9	-5.5	13.3	13.9

δ^{13}Cc: carbon isotope composition of apatite carbonate

δ^{13}Cdiet: calculated carbon isotope composition of the vertebrate diet

Δ^{13}C leaf: δ^{13}Ccarb - δ^{13}Cdiet offset value

P: calculated amount of precipitation (mm)

δ^{18}Oc: oxygen isotope ratio of apatite carbonate

δ^{18}Op calc.: calculated oxygen isotope composition of apatite phosphate

δ^{18}Osw: oxygen isotope composition of Atlantic oceanic surface waters during the LGM

δ^{18}Ow cor. Ice (+1.2): calculated oxygen isotope composition of vertebrate diet water corrected from contiental volume ice (corresponding to a δ^{18}Osw = +1.2‰)

δ^{18}Ow cor. Ice (+0.8): calculated oxygen isotope composition of vertebrate diet water corrected from contiental volume ice (corresponding to a δ^{18}Osw = +0.8‰)

T (δ^{18}Osw = +1.2): calculated mean air temperature assuming a δ^{18}O of +1.2‰ for the oceanic surface waters

T (δ^{18}Osw = +0.8): calculated mean air temperature assuming a δ^{18}O of +0.8‰ for the oceanic surface waters

	MAP (mm)	MAP* (mm)	P (S.D.) (mm)	δ^{18}Ow ‰ VSMOW (δ^{18}Osw = +1.2)	δ^{18}Ow ‰ VSMOW (δ^{18}Osw = +0.8)	δ^{18}Ow (S.D.) ‰ VSMOW	MAAT (°C)	MAAT (S.D.) (°C)	T-EUROPE (°C) Skrzypek et al. 2011 (δ^{18}Osw = +1.2)	T-EUROPE (°C) Skrzypek et al. 2011 (δ^{18}Osw = +0.8)	S.D.	MAT anomaly (°C) (δ^{18}Osw = +1.2)	MAT anomaly (°C) (δ^{18}Osw = +0.8)	MAP anomaly (mm)
Modern meteo data for cities close to the archaeological sites:														
Almeria	202.0	N/A	66.2	-5.8		1.2	19.2	0.4						
Cestas-Pierroton	937.3	N/A	191.5	-5.8		0.7	13.1	0.6						
Santander	1049.9	N/A	140.3	-5.8		0.3	14.8	0.4						
Valencia	531.7	N/A	172.9	-5.2		0.7	18.5	0.6						
MAP, MAT and their anomalies relative to present-days calculated for the studied archaeological sites:														
Nerja (≈Almeria)														
Capra	78	228	16	-5.8	-5.4	0.8	N/A	N/A	13.4	14.0	1.1	-5.8	-5.2	-125
Laugerie-Haute (≈ Cestas)														
Caprinae	118	268	48	-10.4	-10.0	1.2	N/A	N/A	6.9	7.5	1.7	-6.2	-5.6	-819
Caprinae	120	270	39	-9.8	-9.4	0.5	N/A	N/A	7.8	8.4	0.7	-5.3	-4.7	-818
Equus	245	395	42	-11.9	-11.5	0.7	N/A	N/A	6.5	7.1	0.9	-6.6	-6.0	-693
Caprinae	105	255	n.a.	-11.7	-11.3	n.a.	N/A	N/A	5.1	5.7	N/A	-8.0	-7.4	-833
Rangifer tarandus	172	322	37	-10.8	-10.4	1.0	N/A	N/A	6.4	7.0	1.5	-6.7	-6.1	-765
Malladetes (≈Valencia)														
Capra	121	271	42	-5.4	-5.0	0.8	N/A	N/A	14.0	14.6	1.1	-4.5	-3.9	-411
El Cierro (≈ Santander)														
Cervus elaphus	363	513	79	-10.0	-9.6	0.6	N/A	N/A	7.6	8.2	0.8	-7.2	-6.6	-687
Capra	194	344	16	-10.8	-10.4	0.3	N/A	N/A	6.4	7.0	0.4	-8.4	-7.8	-856
Cervus elaphus	323	473	50	-10.1	-9.7	0.2	N/A	N/A	7.4	8.0	0.3	-7.4	-6.8	-727
Capra	169	319	n.a.	-11.2	-10.8	n.a.	N/A	N/A	5.8	6.4	N/A	-9.0	-8.4	-881
El Pendo (≈ Santander)														
Cervus elaphus	270	420	26	-9.8	-9.4	0.3	N/A	N/A	7.8	8.4	0.5	-7.0	-6.4	-780
El Ruso (≈ Santander)														
Cervus elaphus	310	460	156	-8.5	-8.1	0.7	N/A	N/A	9.6	10.2	0.9	-5.2	-4.6	-740
Hornos de la Pena (≈ Santander)														
Cervus elaphus	380	530	n.a.	-11.2	-10.8	n.a.	N/A	N/A	5.9	6.5	N/A	-8.9	-8.3	-670
Capra & Rupicapra	157	307	43	-10.8	-10.4	0.9	N/A	N/A	6.3	6.9	1.3	-8.5	-7.9	-893
Equus	307	457	11	-11.1	-10.7	0.4	N/A	N/A	7.5	8.1	0.6	-7.3	-6.7	-743

MAP = Mean Annual Precipitation in mm
MAP* = Mean Annual Precipitation in mm corrected from the LGM pCO_2 estimate
δ^{18}Ow = mean oxygen isotope composition of precipitations
δ^{18}Osw = mean oxygen isotope composition of oceanic surface waters
MAAT = Mean Annual Air Temperatures obtained from IAEA/WMO database
MAT = calculated Mean Air Temperatures at archaeological sites
MAT anomaly = anomaly in MAT relative to present-days
MAP anomaly = anomaly in MAP relative to present-days